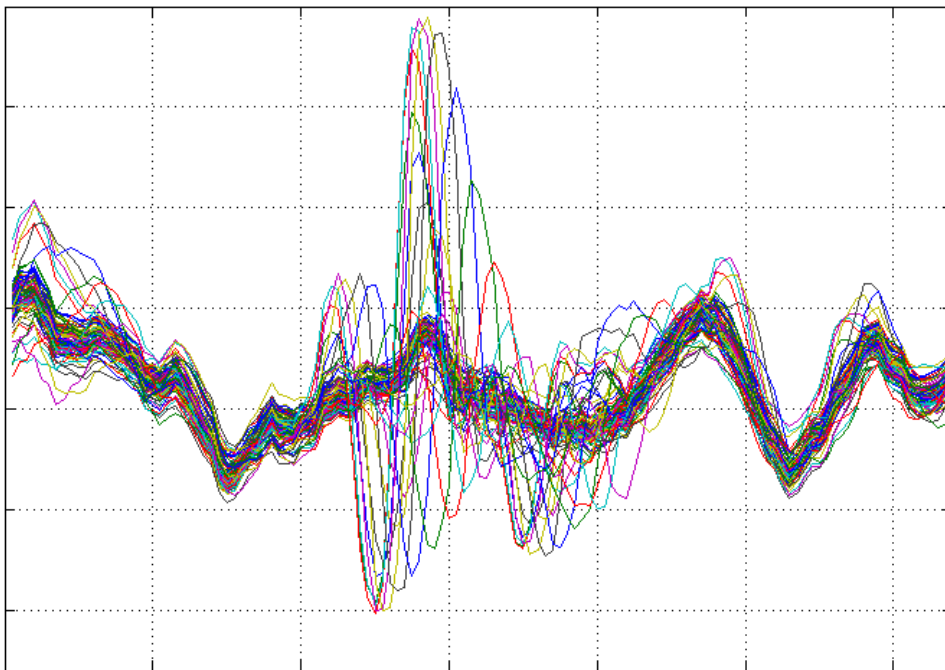


CHALMERS



Development of Signal Processing Algorithms for a new Ultra-wide band Radar System using UWB CMOS chip

Master of Science Thesis in Signals and Systems

YINAN YU

Department of Signals and Systems
CHALMERS UNIVERSITY OF TECHNOLOGY
Göteborg, Sweden 2011
Report No. EX008/2011

MASTER'S THESIS 2011

Development of Signal Processing
Algorithms for a new Ultra-wide band Radar
System using UWB CMOS chip

YU YINAN

Department of Signal and Systems
CHALMERS UNIVERSITY OF TECHNOLOGY
Göteborg, Sweden 2011

Ultra-wide band radar signal processing

© YU YINAN, 2011

Master's Thesis 2011:EX008

Department of Signal and Systems
Chalmers University of Technology
SE-41296 Göteborg
Sweden

Tel. +46-(0)76 582 5672

Ultra-wide band radar signal processing
Master's Thesis in the Master's programme in Communication Engineering
YU YINAN
Department of Signal and Systems
Chalmers University of Technology

Abstract

In this thesis, signals from a new prototype of Ultra Wide Band (UWB) radar transceiver system based on CMOS technology has been introduced and analyzed. The received signal is modeled as three additive parts: the clutters, the reflections from the targets, and the noise. The goal of the signal processing algorithm development is to retrieve the signal of interest by eliminating the unwanted signal components and implement functionality of this radar system. The main functions which have been proposed in this thesis work are system calibration, clutter map estimation, adaptive thresholding, ranging and tracking. Both theoretical derivations and practical implementations are presented. The results have been evaluated in different scenarios and a demonstration of the Graphic User Interface (GUI) control is given in the end of the thesis.

Keywords: UWB radar, clutter, noise reduction, ranging, tracking

Contents

Abstract	iii
Contents	iv
Acknowledgements	vii
1. Introduction	1
1.1. R2A Ultra Wide Band radar chip	1
1.1.1. System parameters	4
1.2. System issue and task description	4
1.3. Accomplishment	8
2. System modeling	11
2.1. Clutter Matrix	14
2.2. Object Matrix	16
2.3. Noise Matrix	16
3. Adaptive clutter map and thresholding	17
3.1. Theory	17
3.1.1. Clutter map generation	17
3.1.2. Noise estimation and thresholding	21
3.2. Measurement result and evaluation	25
3.2.1. Clutter estimation	25
3.2.2. Thresholding	29
3.3. Conclusion	31
4. Ranging	33
4.1. Notation	33
4.2. Theory	34
4.2.1. Pulse locating	34
4.2.2. Sub-sample resolution and differential ranging	50
4.2.3. Multi-target Locating	51
4.2.4. Calibration	51
4.3. Method and Evaluation	54

4.3.1. Evaluation of the pulse locating approaches	54
4.4. Conclusion	65
5. Tracking	67
5.1. Theory	67
5.1.1. Kalman filter for one dimensional tracking	67
5.1.2. Two dimensional tracking	69
5.2. Evaluation and results	72
5.3. Conclusion	77
6. Examples and Demonstration	79
6.1. Set parameter	79
6.2. Tests	81
6.2.1. Raw data	81
6.2.2. Differential ranging	83
6.3. Functions	84
6.3.1. Calibration	84
6.3.2. Clutter estimation	84
6.3.3. Ranging	84
6.3.4. Tracking	88
7. Conclusion and future work	95
References	97
A. Kalman filter for 2D tracking	99
A.1. Initialization	99
A.2. Kalman equation	100

Acknowledgements

I would like to thank every person from Chalmers University of Technology and IMEGO Institute who supports me on this thesis work:

- Firstly my thesis supervisor Professor Tomas McKelvey, who not only gave me great ideas on the thesis work, but also the philosophy of scientific research in general;
- Deepest gratitude to Docent. Jian Yang, without whose professional advises and encouragement, this project would not have been possible;
- Kenneth Malmstrom, my supervisor from IMEGO Institution, who is an insightful person that always gave me pertinent suggestions on different aspects;
- Dr. Borys Stoew and Dr. Peter Bjorkholm from IMEGO who helped me greatly;
- Eventually special appreciation for my father and my boyfriend, who are both always strict and push me forward.

1. Introduction

The objective of this thesis project is to develop signal processing algorithms for a new Ultra-wide band radar system with the Novelda Ultra-wide band radar chip R2A. Details about the radar system can be found in reference [1], and only the general idea will be introduced in this section.

1.1. R2A Ultra Wide Band radar chip

Basically, the R2A system is a pulse radar system shown in Figure 1.1 - it is sending out pulses using one antenna and receiving by the other. The received signal is the transmitted signal bouncing back from objects viewed by the transceiver; it could be considered as a filtered version of the transmitted signal. This echo contains the reflections from near field environment along with the target. A target is usually considered to be a moving object within the radar field.

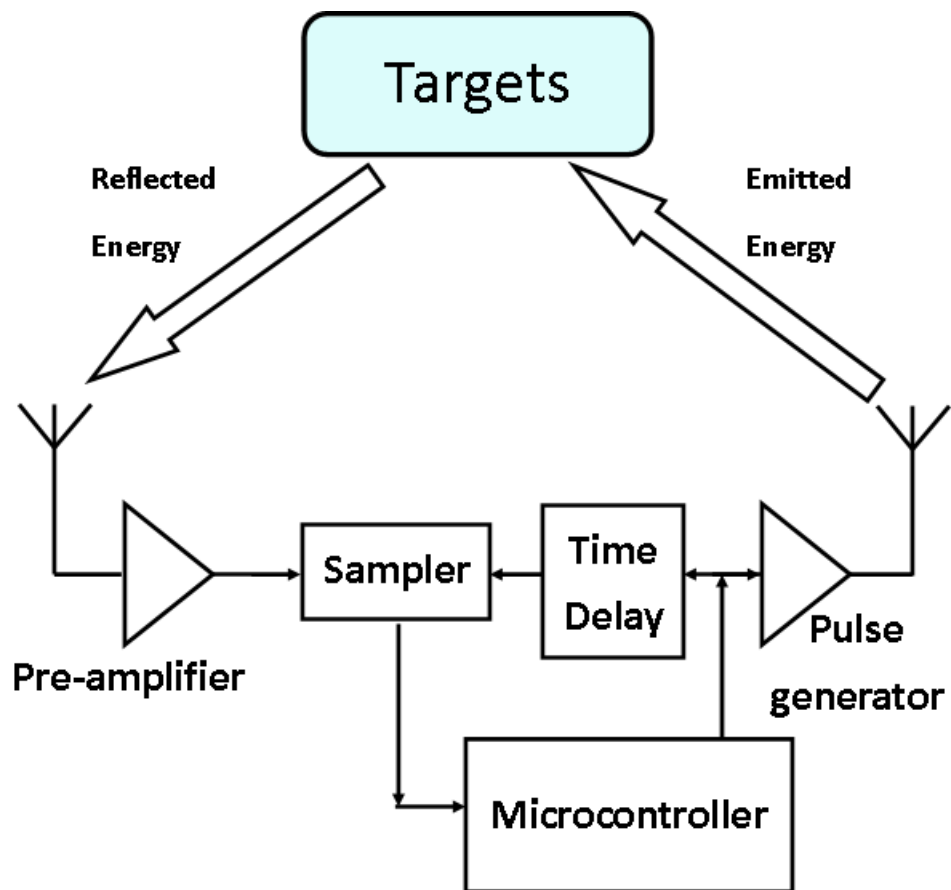


Figure 1.1.: The figure shows how the R2A radar system works. As a traditional radar system, the energy is sent out by one antenna and the reflection is received by the receiver.

For memory efficiency, each measurement is taken within a window set up by a pre-defined time delay. The time delay is called Frame Offset (FO). One window is called one frame and within each frame there are 128 samples. The time delay between every consecutive two samples is approximately 27.8 ps. Converted to spatial domain, this 27.8 ps delay represents approximately 4.5 mm. Therefore in each frame, the duration of the signal is $127 \times 27.8 \text{ ps} = 3.53 \text{ ns}$ in time and approximately 550 mm in spatial domain.

The important parameters are introduced in Section 1.1.1.

1.1.1. System parameters

The most important parameters and their properties are presented in Table 1.1.

According to the parameter settings explained in Table 1.1, before the transmitter sending out a pulse, 1000 (AF) pulses are averaged internally to obtain a less noisy output. The Pulse Repetition Frequency (PRF) of the output signal is 48 MHz, which means the time interval between two consecutive transmissions is $\frac{1}{48\text{MHz}}$ sec. After the signal is transmitted, the receiver will wait for roughly $400 \times 27.8 \approx 11092$ ps before it starts to sample the reflected signal. This waiting time is determined by the parameter Frame Offset (FO) which is set to be 400 samples. In space, it is a distance of approximately 3.3 m away from the radar chip (regardless of the cable connecting the antenna and the radar chip). Therefore, in spatial domain, one received signal is taken within a window spans the range 3.3 m to $3.3 + 0.55$ m, since the window size of the measurement is roughly 0.55 m.

1.2. System issue and task description

For this UWB radar system shown in Figure 1.2, we face specific challenges introduced as below:

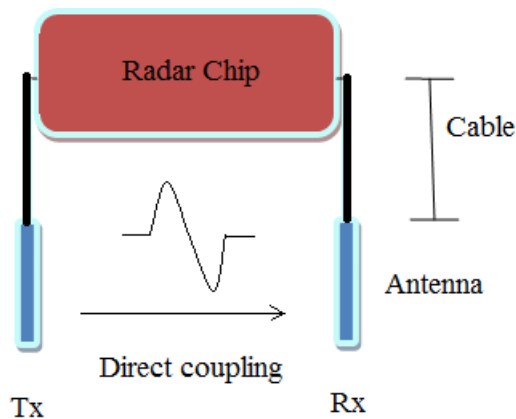


Figure 1.2.: The UWB radar system. The red box indicates the radar chip. The black lines denote the cables connecting the chip and the antennas. The signal from the transmitter (Tx) to the receiver (Rx) is the direct coupling between the two antennas.

- Near field issue:

Table 1.1.: Introduction of the important parameters for the UWB radar system.

Parameter	Description	Default Value
Chip Number (CN)	The identification of different radar chip. Each radar chip has a different pulse template (see Chapter 4).	3000109
Port Name (PN)	The port that connects the radar chip and the computer. It needs to be set up correctly.	'COM6'
Averaging Factor (AF)	How many internal signals are taken before output, which effects the processing speed and the noise level.	1000
Frame Offset (FO)	Internal time delay: decides the range of the view for the radar	400
Pulse Repetition Frequency (PRF)	By which frequency the pulses are sent out	48 MHz
Gain	The gain of the transmitted signal.	1
Zoommin/Zoommax	The zoom value of the received signal.	0/100

Since we are working in the near field, the received pulse duration is not negligible compared to the range to the target, and therefore, the variation of the pulse shape is relatively significant, which raises problems for the pulse locating procedure. Instead of traditional spatial matched filter [4], we need to deal with a distorted template matching problem.

- Direct coupling and disturbance:

The direct coupling between the two antennas should not be ignored. This might introduce a disturbance to our signal analysis. After carefully examining the properties of this unwanted signal, we need to get rid of its contribution. As will be illustrated in Chapter 4, the direct coupling can be used for system calibration.

- Temperature dependence:

The ranging measurement of this system is based on the samples unit. The sample interval Δ_s together with the number of samples N_s describe the time delay between the transmitted pulse and the received pulse. The sample interval Δ_s is the distance between each two consecutive samples it represents in spatial domain. As has been discussed above, there are 128 samples in one measurement, and the time interval between two consecutive samples is roughly 27.8 ps.

Therefore the range d could be written as:

$$d = \frac{\Delta_{s1}j_1 + \Delta_{s2}j_2}{2} \quad (1.1)$$

where Δ_{s1} is the sample interval when the pulse travels in the air and Δ_{s2} represents the sample interval in the cables shown in Figure 1.2, and thus N_{s1} and N_{s2} are the corresponding sample indices at which the target locates respectively. From experiments we know that the speed Δ_{s2} is relatively constant. So we have:

$$\Delta_{s2}j_2 \approx c \quad (1.2)$$

where c is a constant value indicates the length of the two cables.

However, since the system is temperature dependent, the Δ_{s1} is not a fixed parameter. To obtain the accurate distance, we need to calibrate the system for each new measurement.

- Clutter:

The clutter is defined as the reflection from the environment, instead of the real target. Normally in a radar application, the desired signal is the echo from the moving target, so that we need to suppress the unwanted part in the received signal, in order to retrieve the 'real' signal for either ranging or further analysis.

- Noise:
Noise and disturbance are interpreted as the random part of the received signal, which needs to be estimated and suppressed as much as possible.
- Jamming:
Jamming is the signal generated from other sources, mixed in the receiver. However, it is not within the scope of this thesis.

Therefore, the work is divided into three parts:

- System and signal analysis:
 - With limited prior knowledge, try to understand the behavior of the system;
 - Measure and analyze both the generated and the received signal;
 - Identify the different parts of the received signal.
- Solution to system issue:
Including clutter map generation, noise reduction, calibration, near-field compensation. In this case, clutter and noise are both defined as 'unwanted direction' in the vector space, which are suppressed accordingly.
- Algorithm design: Theoretical and practical algorithms development for possible applications, not only to obtain working functionalities, but also to achieve a promising theoretical result.

1.3. Accomplishment

The main achievement is briefly listed as below.

- Adaptive clutter map and thresholding (Chapter:3):
An SVD-based clutter rejection and thresholding technique has been applied, and an optimal clutter map estimation has been achieved.
- Calibration (Chapter:4):
Since the system is temperature dependent, an adaptive calibrating method is applied, which is based on the direct coupling measurement. The prior knowledge of the radar system is updated for each new measurement according to this calibration result.
- Ranging (Chapter:4):
Five different pulse locating techniques have been applied to this 'distorted template matching' problem. Sample-based pulse locating and subsample resolution for differential ranging are achieved accordingly.
- Tracking (Chapter:5):
Measurement for tracking requires a fast and reliable algorithm and a Kalman filter is employed to correct the result in real time according to least square criterion. One dimensional and two dimensional tracking has been achieved.

The functions have been developed and implemented in this thesis work are summed up in Figure 1.3.

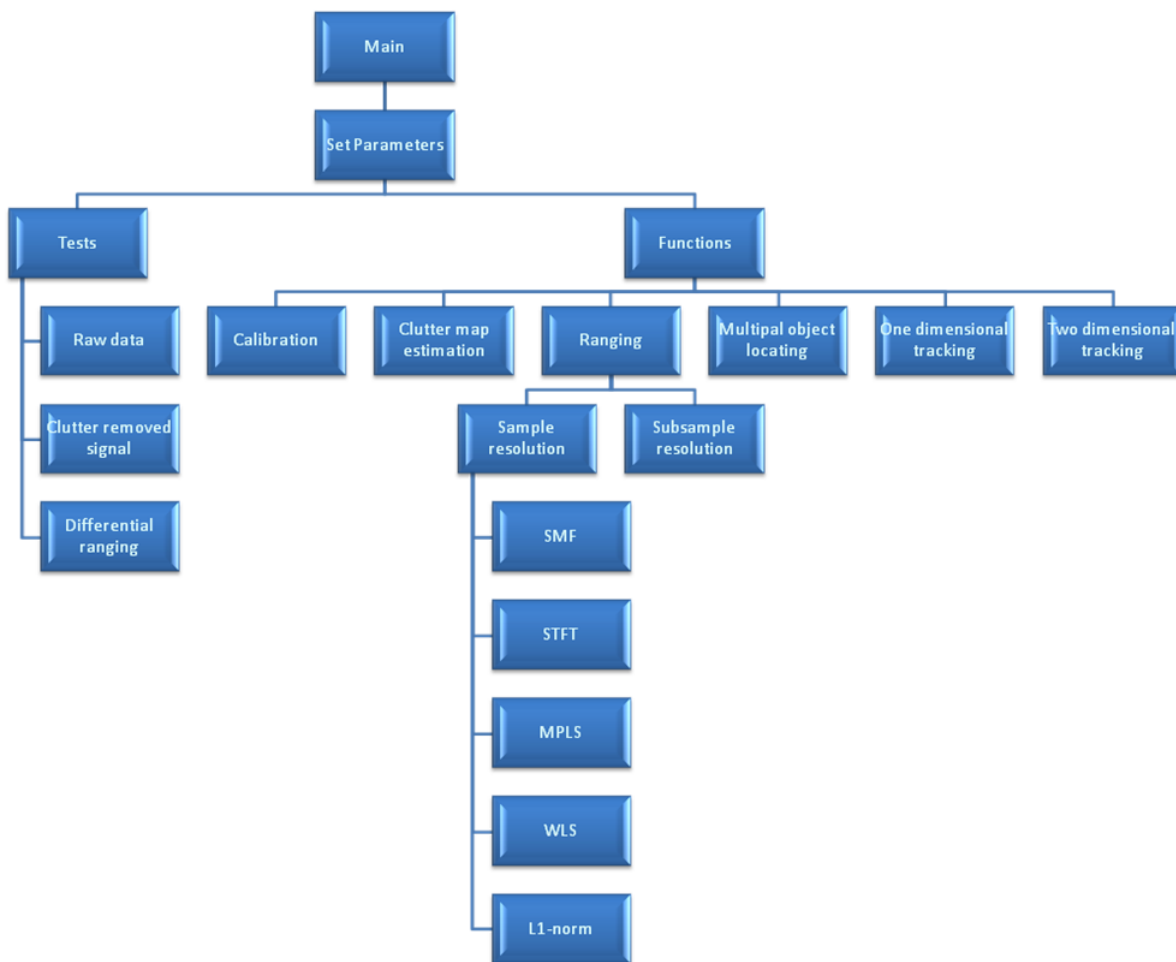


Figure 1.3.: A demonstration of the working functions implemented in this thesis project.

2. System modeling

In this chapter, the modeling of the system is described in detail.

One example of received signal r is shown in Figure 2.1. And as shown in Figure 2.2, this signal r consists of the clutters r_e , the signal reflected from the target r_o and the noise e . Here we assume that there is no jamming, namely no other source that produces microwave signals.

The signals r , r_e , r_o and e are represented as 128 dimensional column vectors, since there are 128 samples in each received signal.

The clutter r_e is considered as a summation of the received reflections, namely the superposition of the reflected pulses with different amplitudes and phases. Among all the objects in the radar field, one or one type of objects with some properties in common are defined as the target of interest. The reflections from these targets r_o are the signals we are concerned about.

In Figure 2.1, r_o is considered as the reflection from a moving plate with 500×250 mm^2 area. The plate is made of metal which causes a strong reflection. The noise r_e is estimated in Chapter 3.

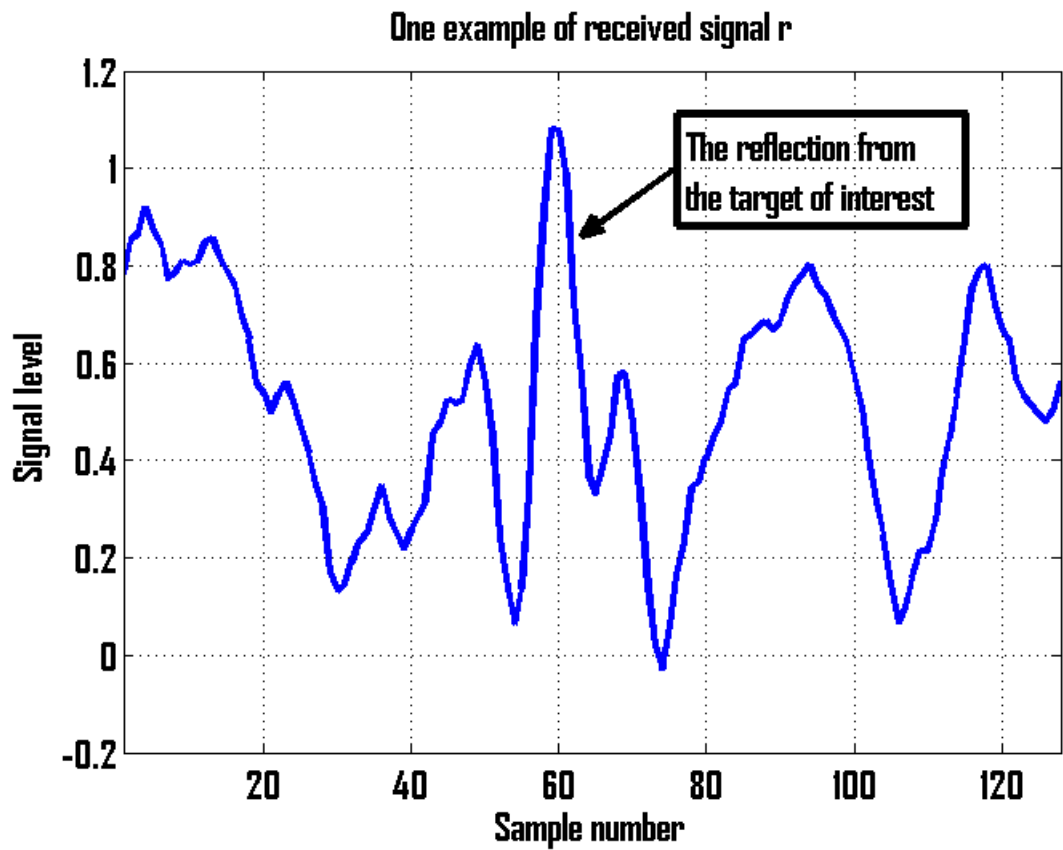


Figure 2.1.: One example of the received signal r . The target of interest is a metal plate with $500 \times 250 \text{ mm}^2$ area which provides the strongest echo compare to all the other echoes bouncing back from the environment. This reflection is called r_o and is shown as the outstanding signal labeled in the figure. There are 128 samples in this signal. The signal level shown in this figure is a number which is proportional to the voltage of signal at each sample and represents the superposition of the reflected energy from all the objects.

So one measurement is structured as:

$$r = r_e + r_o + e, \quad (2.1)$$

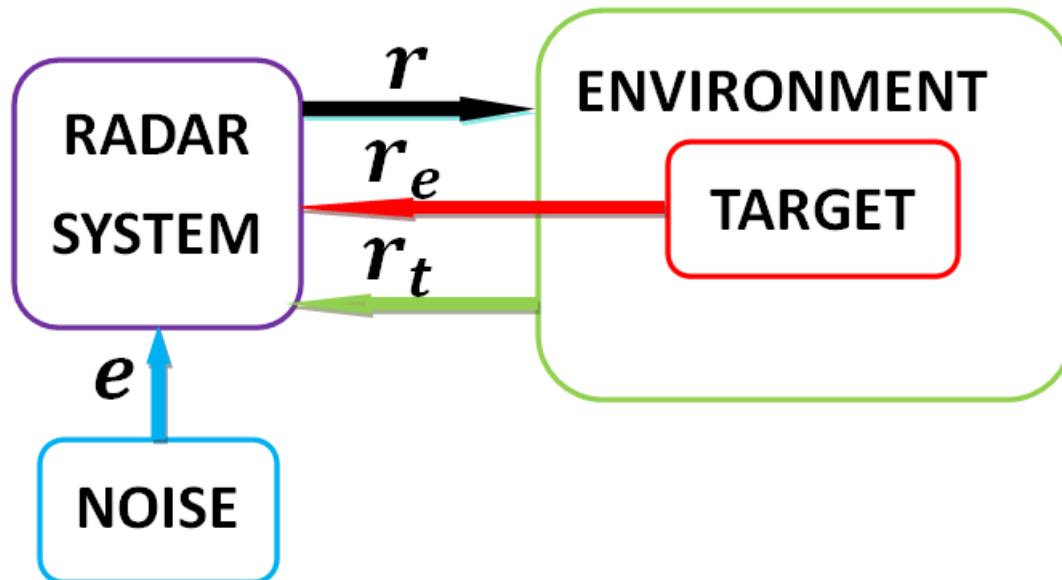


Figure 2.2.: The radar system and the components of the received signal. The purple box indicates the radar system shown in Figure 1.2 and additive noise is added. The reflection consists of r_e the clutter, r_o the reflection from the target, and e the noise.

If the vectors r^1, r^2, \dots, r^n denote the consecutively received signals at time i , a measurement matrix X could be formed as:

$$X = [r^1, r^2, r^3, \dots, r^n] \quad (2.2)$$

Now we re-write our measurement matrix X as below, and the upper index i also denotes the time index in each each matrix:

$$\begin{aligned} X &= X_e + X_o + E \\ &= [r_e^1, r_e^2, \dots, r_e^n] + [r_o^1, r_o^2, \dots, r_o^n] + [e^1, e^2, \dots, e^n] \end{aligned} \quad (2.3)$$

It shows that the measurement matrix is written as a summation of clutter measurement matrix X_e , object matrix X_o and noise matrix E .

For each matrix defined above, individual analysis is presented in the following sections.

2.1. Clutter Matrix

Clutter, for indoor applications, can be defined differently according to different objectives. Without loss of generality, we define clutter as the relative static indoor environment for applications of detecting moving objects.

According to further analysis, each clutter measurement r_e^i could be written as a linear model:

$$r_e^i = \alpha_i r_c + c^i \quad (2.4)$$

which is a re-scaled version of the vector which represents the 'clutter direction' with a bias c^i .

Therefore, the clutter matrix $X_e = [r_e^1, r_e^2, \dots, r_e^n]$ could be further expressed as:

$$X_e = [\alpha^1 r_c + c^1, \alpha^2 r_c + c^2, \alpha^3 r_c + c^3, \dots, \alpha^n r_c + c^n] = R_c + C \quad (2.5)$$

where α^i is the scalar, r_c is the clutter direction in the vector space, and c^i is a vector of ones scaled by a scalar for each measurement i .

Moreover, we can see from this model that the clutter matrix is a rank two matrix shown as in Figure 2.3 since the columns of the matrices R_c and C are linearly dependent.

$$X_e = [\alpha^1 r_c, \alpha^2 r_c, \dots, \alpha^n r_c] + [c^1, c^2, \dots, c^n]$$



Figure 2.3.: The clutter matrix X_e could be written as a summation of two rank one matrices.

2.2. Object Matrix

The reflection from the target is the signal to be obtained and analyzed. One example is shown in Figure 2.4, which is obtained in an anechoic chamber.

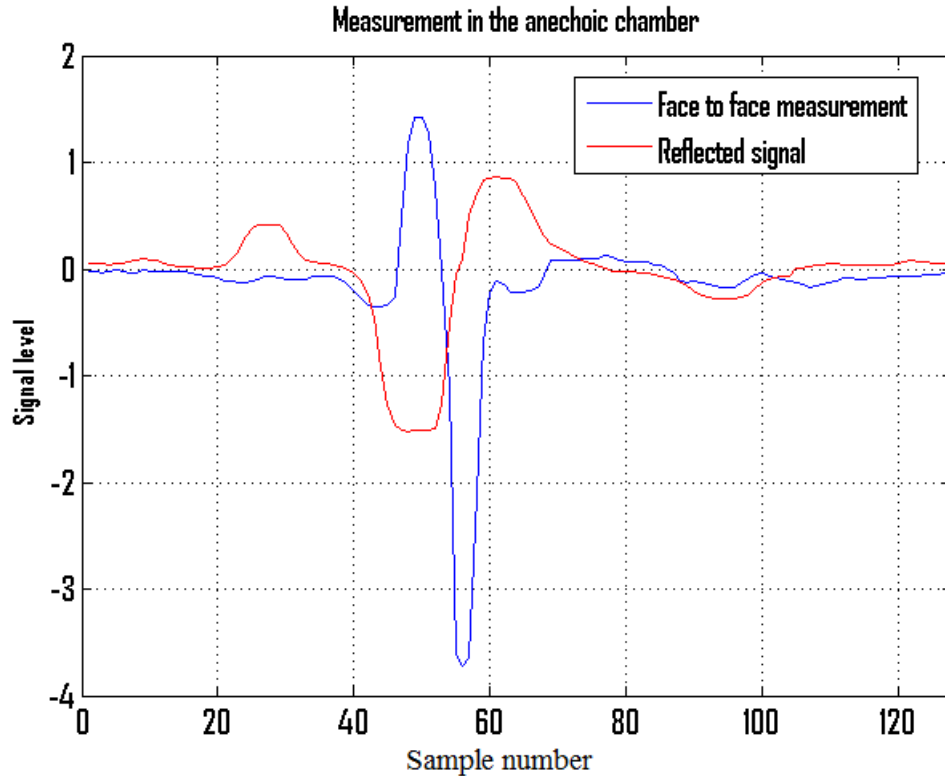


Figure 2.4.: The measurement taken in the anechoic chamber. The blue pulse is taken by face to face antenna measurement with a 140 millimeter distance. The red curve indicates the reflected signal from a metal ball with 100 mm diameter placed in front of the antennas with 70 millimeter range.

2.3. Noise Matrix

Noise is assumed to be additive and defined to be the completely random part which is represented by the vectors with random directions and relatively low power.

Note that in later chapters when we talk about the 'direction', it means the direction of a signal in the vector space.

3. Adaptive clutter map and thresholding

Before we start this chapter we have to establish the definition of what clutter is in one specific radar application. For example, clutter can be defined as the reflections from the environment other than the moving target. Of course, 'unwanted reflection' is a relative concept; it very much depends on what the application is. In this project,

for indoor tracking application, clutter is the reflections from the constant environment, such as furniture or walls. On the other hand, if the aim is to monitor the heart beat from a patient, clutter is defined as everything but the heart beat patterns.

Therefore, the clutter could be either constant (fixed radar with moving object), or varying with time (heart beat monitor with moving carrier); could be strong (in a complex environment) or weak (in an anechoic chamber).

It is very important to suppress the clutter in order to have a functional radar system with high performance under dynamic signal level.

3.1. Theory

3.1.1. Clutter map generation

Direct Mean Method

In the signal model introduced in equation 2.1, the reflection from the target r_o could be considered as a zero-mean random variable if the object is assumed to be moving in a random manner and thus a simple estimation of the environment could be obtained by:

$$\hat{r}_e = \sum_{i=1}^n r^i \quad (3.1)$$

The signal could then be retrieved by:

$$\hat{r}_o = r - \hat{r}_e + e \quad (3.2)$$

which gives the simplest, although not the most efficient clutter rejection result, since the assumption that the reflection of the moving object is a zero-mean random variable does not hold precisely. Therefore, normally when we estimate the clutter by Direct

Mean Method, we also rule in the reflection from the target by averaging the entire signal.

Singular Value Decomposition

Derived from the definition and properties of clutter, a clutter removal method based on Singular Value Decomposition would be a suitable technique for this particular task.

Singular Value Decomposition (SVD) is one of the most powerful matrix factorization methods. It applies to any rectangular matrix and is widely used in engineering problems.

The definition and some essential properties of SVD are briefly introduced in this thesis and more details could be found in reference [3].

Definition of SVD:

Suppose matrix X is full rank with size $m \times n$ ($m > n$) we could factorize X as follows:

$$X = U\Sigma V^H = U \begin{pmatrix} \sigma_1 & \cdots & 0 \\ \vdots & \ddots & \vdots \\ 0 & \cdots & \sigma_r \\ 0 & \cdots & 0 \\ \vdots & \ddots & \vdots \\ 0 & \cdots & 0 \end{pmatrix} V^H \quad (3.3)$$

where U is an $m \times m$ unitary matrix, Σ is an $m \times n$ matrix with nonnegative real numbers as entries, and V is a $n \times n$ unitary matrix. The non-zero entries σ_i of Σ are sorted in a descending order, which are defined as the singular value of matrix X .

As introduced in Chapter 2, the system model defined in equation 2.3 shows how the measurement matrix X is structured: the clutter matrix is approximately a summation of two rank one matrices, which are assumed to be the two stronger rank one matrices in the measurement matrix X . Therefore, one property of SVD, the 'Low Rank Approximation', could be adopted to estimate the clutter map.

The 'Low Rank Approximation' uses the fact that SVD of a rank r matrix could be written as a summation of r rank one matrices:

$$X = \sum_{i=1}^r u_i \sigma_i v_i^H \quad (3.4)$$

- u_i is the i^{th} left eigenvector of X ;
- v_i^H is the i^{th} right eigenvector of X ;
- σ_i is the i^{th} singular value of X .

'Low Rank Approximation' proves that to find an approximation of rank k matrix X_k ($k < r$), which is obtained by minimizing the Frobenius norm of the difference between X_r and X_k , subject to $\text{rank}(X_k) = k$, we simply take the SVD of X_r , and the solution is given by the summation of first k components. Namely:

$$X_k = \sum_{i=1}^k u_i \sigma_i v_i^H \quad (3.5)$$

In this case, the rank k matrix to be estimated is the clutter matrix and $k = 2$. Since the singular values are sorted in a descending order, X_k is therefore corresponding to the summation of the two strongest vector directions.

A general view of the clutter can be examined in Figure 3.1, the columns of a 128×100 measurement matrix have been plotted. The overlapping part in the figure represents the rank 2 clutter matrix.

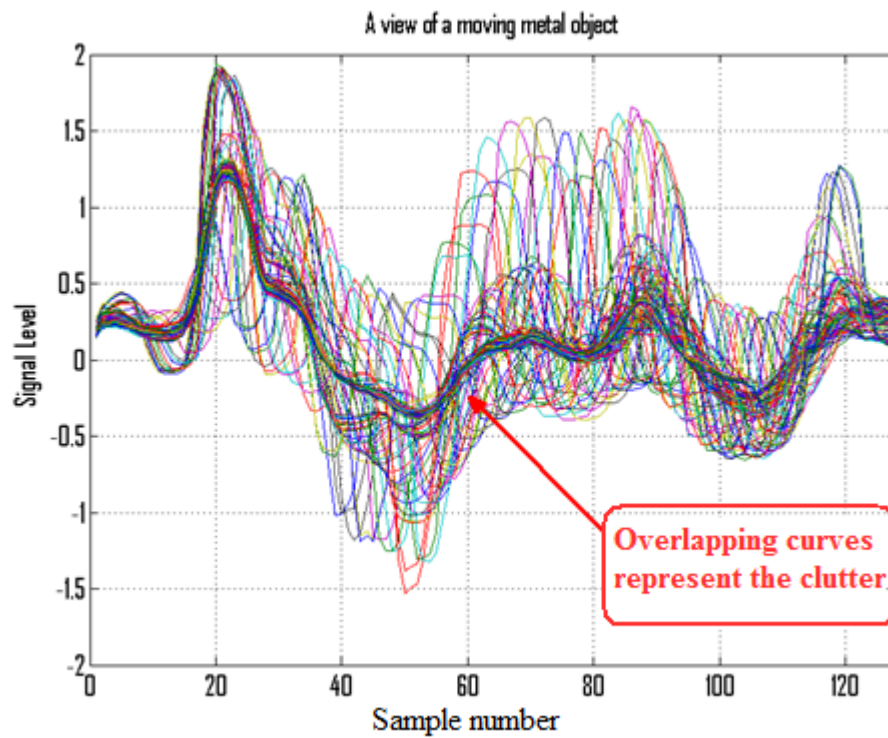


Figure 3.1.: 100 consecutive measurements of moving metal object (225 millimeter by 500 millimeter square) in the presence of clutter.

The number of columns N is the total number of measurements to be put into the measurement matrix X . When N is large, the estimation is more sensitive in the sense that it takes into account a large time interval during which anything that does not move is considered clutter. This is good for the application which requires more sensitive motion detection. In such cases, when any movement occurs from any object, this object should be classified as a target of interest. On the other hand, if N is small, a shorter time interval is measured. In this case, any object that appears to be static for a short time will be considered a part of the clutter map. Therefore, the clutter is defined according to specific applications where we should choose a proper value of N to fulfill our requirements.

The evaluation will be shown in Section 3.2.

3.1.2. Noise estimation and thresholding

Decision for the Frame Offset

The Frame Offset (see Chapter 1) is one parameter to be chosen before starting the system. To choose the value, we have to decide the most probable range which the target is within.

The received signal within the dynamic range (≈ 15 meters) is a vector r which is segmented into approximately 30 frames. The most efficient way is to first determine the most probable location of the target with respect to the frame number and then process the corresponding signal within that frame. To determine this, the energy contained in each frame is compared with the two neighbors as follows:

$$r = [r_1^T, r_2^T, \dots, r_{30}^T]^T \quad (3.6)$$

The energy Egy_{ri} for frame i is defined as:

$$Egy_{ri} = \sum_{k=1}^{128} r_{ik}^2 \quad (3.7)$$

The criteria is:

$$\hat{i} = \arg \max_i \frac{2Egy_{ri}}{Egy_{ri-1} + Egy_{ri+1}} \quad (3.8)$$

Then we consider the i^{th} frame contains the target with a higher likelihood and the Frame Offset will be chosen as:

$$\hat{FO} = 128(\hat{i} - 1) \quad (3.9)$$

Thresholding within one frame

One frame indicates approximately 550mm with 128 samples, which is defined with respect to the memory efficiency for the computer to process with. The thresholding within one frame determines the presence of any moving targets within the field of the radar system. The threshold is decided by comparison of the received echo within one frame determined by the pre-defined Frame Offset and the estimated noise level. If the signal level is larger than the noise, the presence of the target is considered as positive and vice versa.

The noise is defined as the vectors with completely random directions in the signal space with low power. The direction of the Noise Vector could be also estimated by the SVD of X and therefore be used to reduce the effect of noise. Since the small singular values and corresponding singular vectors indicate signals with relatively low power and random vector directions, in the case that without any target, the noise level could be estimated by taking the first 2 rank 1 matrices as the clutter map and the rest of the measurement could be considered as random noise.

According to the model introduced in Chapter 2,

$$X = R_e + N \quad (3.10)$$

where R_e indicates the Clutter Matrix and N is the Noise Matrix.

Therefore, the noise level could be estimated as:

$$\hat{N} = X - R_e \quad (3.11)$$

The estimated noise and its distribution are shown in 3.2 and 3.3 respectively.

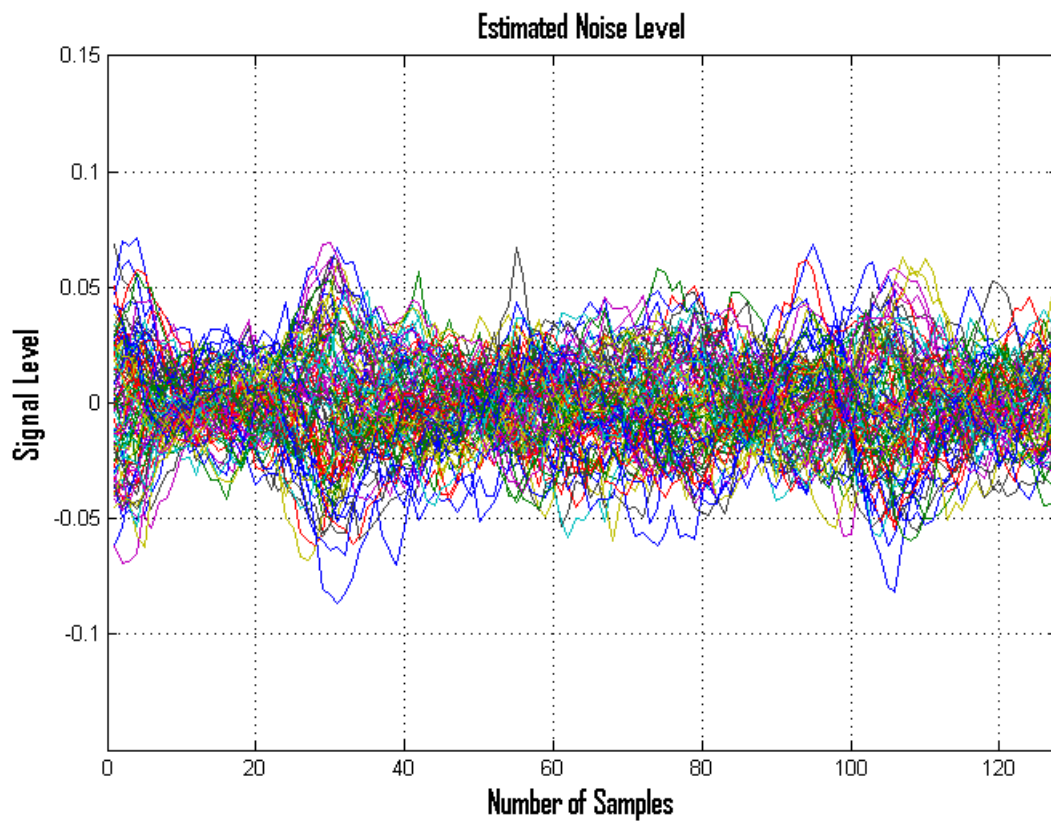


Figure 3.2.: Estimated noise level from the model $\hat{N} = X - R_e$. This is under the parameter setting as Frame Offset = 400, Gain = 1, Averaging Factor = 1000.

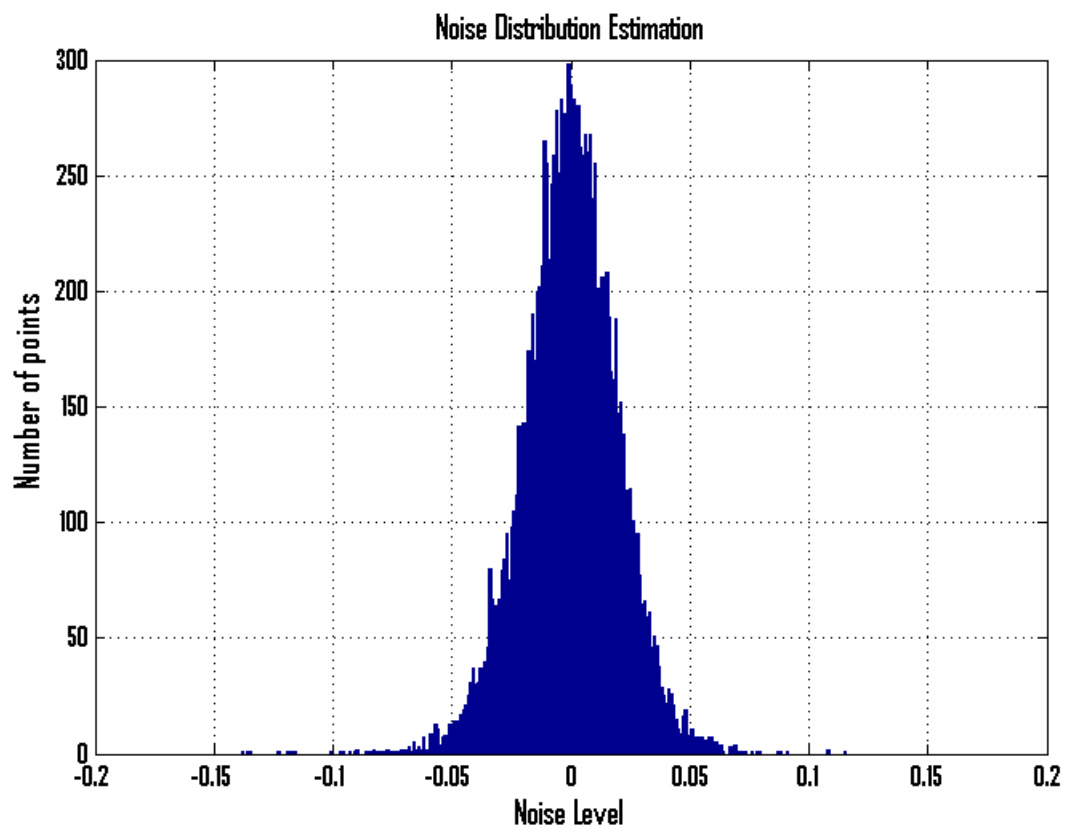


Figure 3.3.: Noise distribution estimated by SVD. It appears to be a zero-mean Gaussian distribution with standard deviation 0.0186.

From the estimation, we can characterize the noise as a zero-mean Gaussian distribution with the standard deviation of 0.0186. Note that this estimation is in the scenario where Frame Offset (FO) = 400, Gain = 1, Averaging Factor (AF) = 1000. When the parameters vary, the noise level will be different. For example, if AF decreases, the noise level will increase accordingly.

From a practical point of view, by this noise level estimation during the clutter map generation, we can estimate the presence of the target by compare the noise level and the signal level of the received echoes.

3.2. Measurement result and evaluation

3.2.1. Clutter estimation

In Section 3.1.1, the Direct Mean Method and SVD based clutter estimation have been introduced and discussed. In this section, we will evaluate and compare the two techniques.

The evaluation on real measurement data could be classified as:

- Clutter estimation without a moving target
- Clutter estimation with a moving target

Without moving objects, the measurement could be considered as a combination of clutter and noise: $X = X_c + E$, which makes the evaluation easier. The estimation result in terms of RMSE of both Direct Mean method and SVD based method are shown in Figure 3.4 which also shows the results obtained by the Direct Mean Method. We can see from the comparison that SVD clutter rejection gives a more promising result.

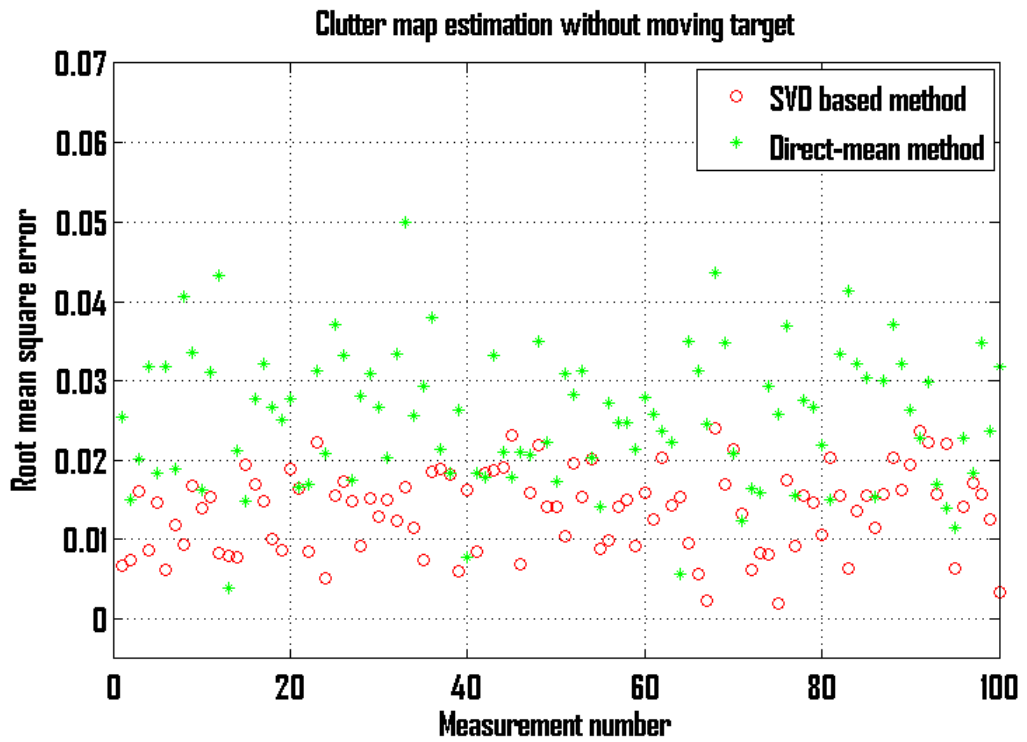


Figure 3.4.: Evaluation comparison between SVD clutter map and averaging clutter map without moving object. The blue and the red dots indicate the RMSE of the SVD estimation and the Direct Mean Method respectively.

In the presence of a moving target, the evaluation becomes more complicated since the measurement is no longer repeatable. Therefore we simulate the signal by adding together a known clutter matrix and a known movement as shown in Figure 3.5. There are 100 columns in each measurement matrix and the result now could be evaluated by simply computing the RMSE between the known clutter measurements and the estimation. The result is shown in Figure 3.6.

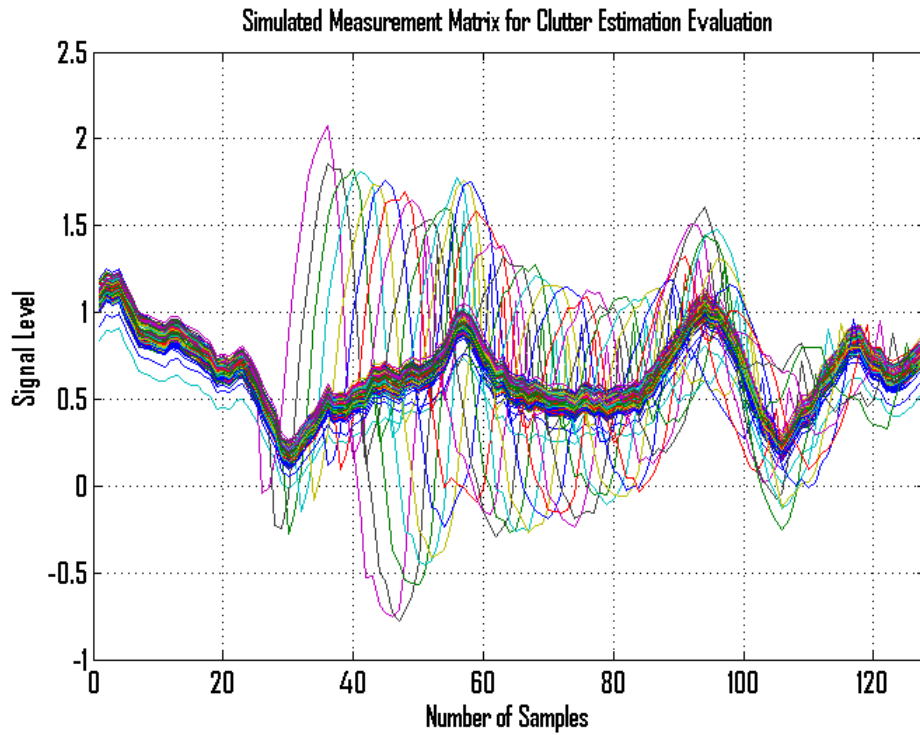


Figure 3.5.: Simulated Measurement Matrix with known clutter map for evaluation. The Clutter Matrix is a Measurement Matrix without moving target.

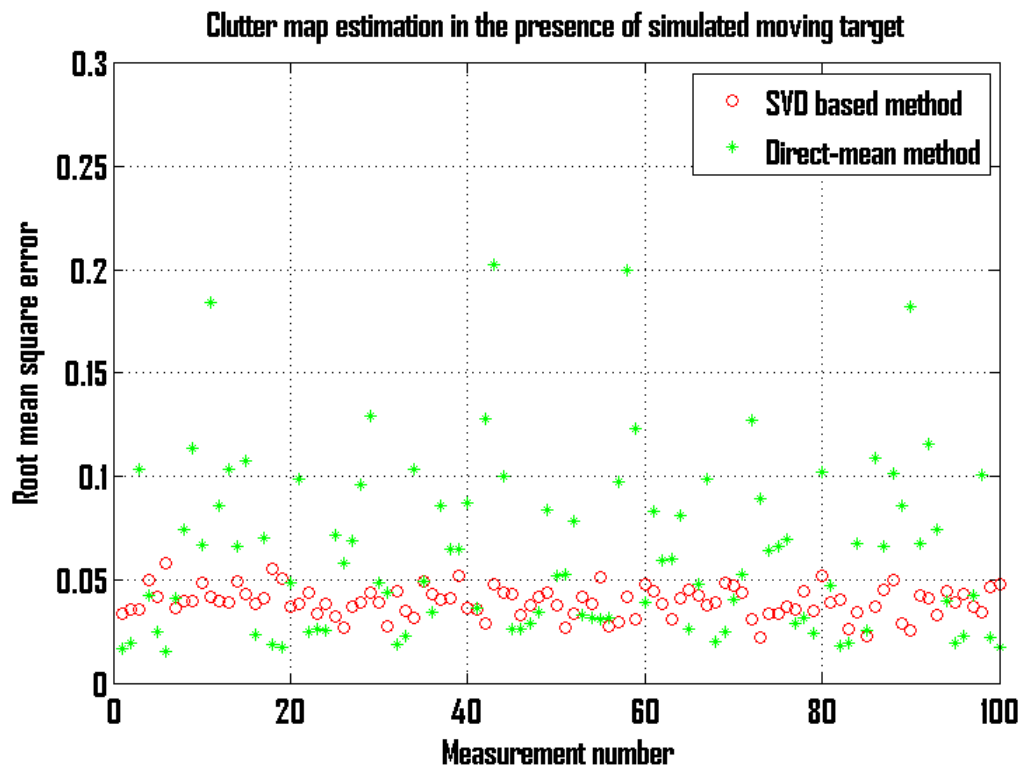


Figure 3.6.: Root Mean Square Error between the known Clutter Map and the estimation.

3.2.2. Thresholding

To evaluate the decision for FO, we change the SNR of the received signal by increasing the noise level. The SNR is defined as:

$$SNR = \frac{A}{\sigma} \quad (3.12)$$

where A is the maximum amplitude of the signal and σ is the standard deviation of the noise.

The evaluation is by the false alarm defined as follows:

$$FLM = \frac{n_f}{n} \quad (3.13)$$

Where n_f is the number of the FO estimations which are wrong and n is the total number of estimations.

This result is shown in Figure 3.7. Each evaluation at the corresponding SNR is based on $n = 40$ independent measurements.

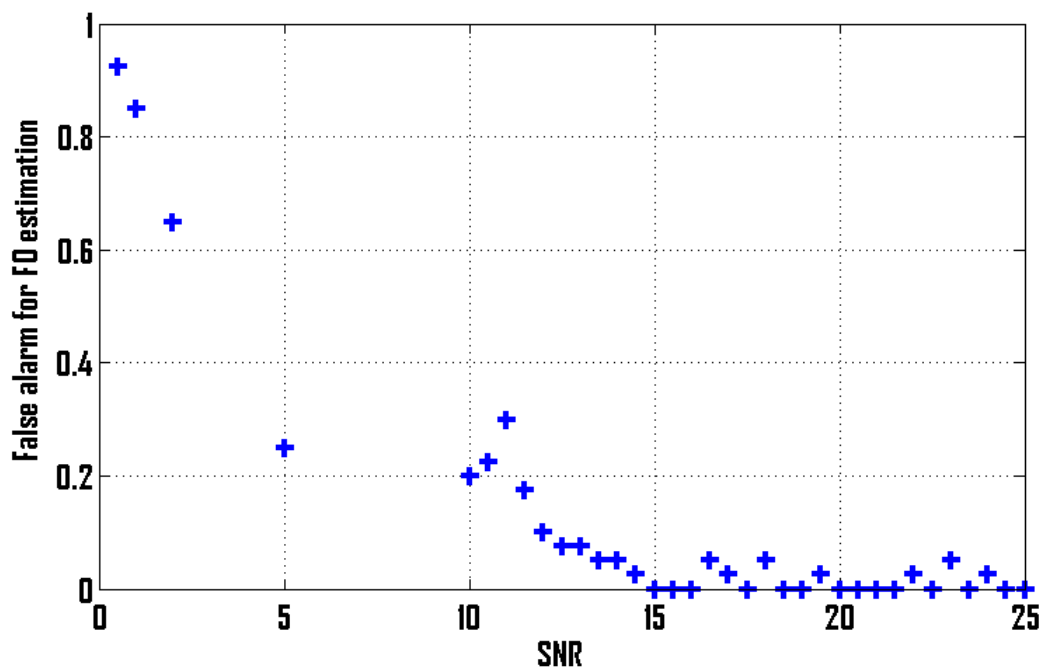


Figure 3.7.: The false alarm for the estimation of the Frame Offset (FO).

The evaluation result for thresholding within one frame is also given by the false alarm defined in Equation 3.13. A Gaussian noise with increasing standard deviation is added onto the received signal to test the robustness of the thresholding algorithm. The results are shown in Figure 3.8.

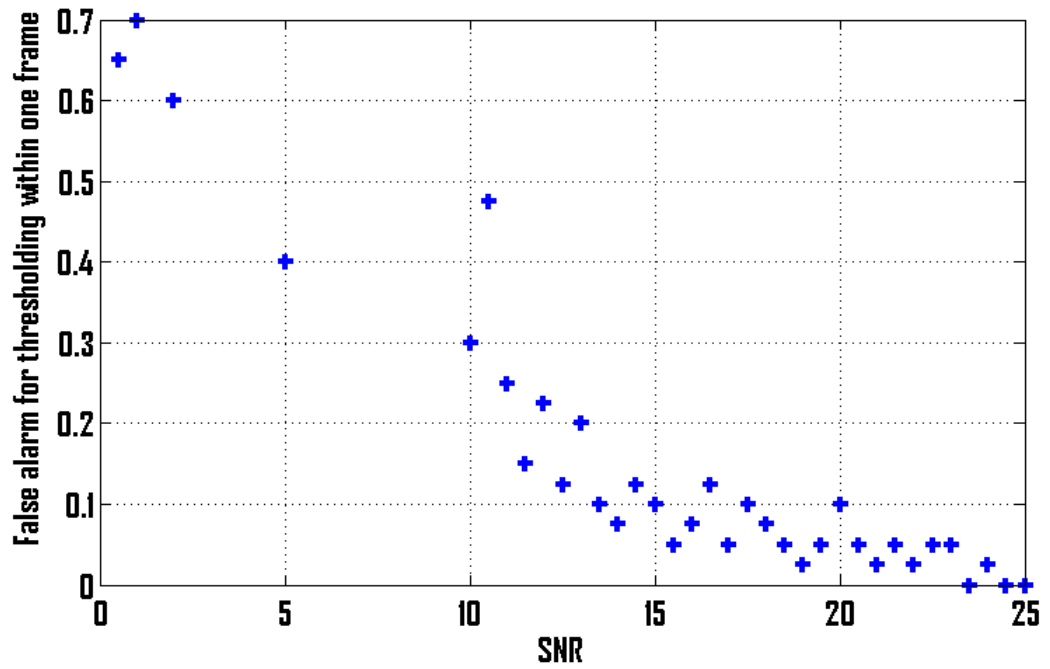


Figure 3.8.: The false alarm for the thresholding within one frame.

3.3. Conclusion

In this chapter, SVD based clutter map estimation and thresholding techniques are introduced and evaluated for simulated signal and real measurement. For clutter estimation, another technique called Direct Mean Method is also implemented and compared with SVD based method. It turns out that the later technique provides a more promising result. A noise Matrix is estimated as the summation of the matrices corresponding to the small singular values. The noise appears to follow a zero-mean Gaussian distribution. Based on these properties, the thresholding methods are developed and shown with efficient results for a reasonable SNR value.

4. Ranging

Ranging, one of the main tasks for traditional radar applications, is discussed in this chapter. Ranging means distance estimation as for radar techniques. The difficulty with respect to the system properties we have talked about in Chapter 1 will be further analyzed and resolved. The structure of this chapter is as follows: in the theory section, five different pulse locating techniques will be theoretically illustrated and compared; then sub-sample resolution is achieved for differential ranging; finally, a robust calibration procedure will be presented to convert the measurement from number of samples to distance, and to get rid of unwanted effects (e.g. temperature dependence). Evaluation and discussion sections are given in the end of this chapter.

4.1. Notation

First, the notations used in this chapter are defined as follows:

Matrices:

- X : the measurement matrix;
- X_c : the clutter matrix;
- X_o : the object matrix, which contains the echoes from the targets;
- E : the noise matrix;

Vectors:

- r : received sequence, with length 128;
- r_c : the vector represents the clutter;
- r_o : the vector represents the reflection from the target;
- e : the noise vector;
- r_m : the 'pulse template', or the pulse signature with length n_w ;
- R : received signal in frequency domain;

- R_m : pulse signature in frequency domain, with length 128;

Indices:

- n : number of measurements contained in the measurement matrix;
- i : index of the signal, $i = 1, 2, \dots, n$;
- k : sample number of the received signal, in time domain or frequency domain; in case of ambiguity, the sample index in frequency domain will be K ;
- n_w : length of r_m , also the window length;
- j : the index of the sample at which the target is located.

4.2. Theory

4.2.1. Pulse locating

To locate the object in one dimension, i.e. ranging, we have to determine the time delay between the transmitted pulse and the received pulse. As introduced in Chapter 1, the system is sample based, and the time delay between two consecutive samples is 27.8 ps. Therefore, the ranging is equivalent to locating the pulse in the received signal with respect to the number of samples, namely, the span of the pulse samples. In this thesis work, five different techniques have been presented and evaluated, which will be discussed in detail as the following order.

- Spatial Domain Signature Matching approach (Matched Filter: MF)
- Short Time Fourier Transform based Signature Matching approach (STFT)
- 'Position Matrix' and Least Square approach (PMLS)
- Weighted Least Square based approach (WLS)
- L1-norm based approach (L1)

Spatial Domain Signature Matching approach

In a radar application, ranging is conventionally done via a spatial domain matched filter, which turns out to be an 'optimal' solution for signal detection within white noise [4] in far field applications, since it maximizes the signal to noise ratio(SNR) in such cases. For our UWB radar system, this approach is also applicable to some extent.

The key concept of spatial matched filter is simply the cross-correlation between the received sequence and a pre-defined template, and therefore matched filter could be also interpreted as a 'template matching' method in the spatial domain. The peak of the correlation coefficients will obviously appear at the point where the pulse is located. There are some requirements though, for example high similarity between the pulse received and the template we have been using. If we are working in far field, the distance between the transceiver and the object is much longer than the pulse duration such that the changes of the pulse signature over transmitting time could be ignored, and therefore the received signal and the template could be considered as approximately identical. Otherwise, the reflection from the target could be considered as having a filtered pulse shape compared to the generated pulse. In this project, since we are working in near field and the object is unknown, to maintain the generalization, the template we use is an averaged version of several reflected pulse signatures from 20 different targets in the anechoic chamber. Of course, there are other ways to modify the template in order to obtain a better result from different viewpoint, whereas signature analysis is another topic which is not within the scope of this thesis work.

To formulate this procedure, the main concept is given as follows:

Suppose we have the signal r_o as the reflection after clutter removal, which could be written as:

$$r_o = r_m d^{(j)} \quad (4.1)$$

where $d^{(j)}$ is a delay factor, indicating the position of the pulse in the whole received sequence in terms of the number of samples. The signature template is called 'pulse model' and denoted as r_m and r_m is shown in 4.1 and has properties as follows:

- r_m is formed by 20 reflected pulse signatures in order to maintain generality. The targets are all different in terms of size, material and shape.
- r_m is a part of the pulse, which is chosen in such a way that mainly the main lobe of the pulse is included, because the pulse locating is mainly defined by the main lobe of the pulse. The length of r_m is expressed as n .
- r_m varies for different radar chips. Individual measurement should be done to every chip. However, for simplicity, when we discuss the 'pulse model', we drop the index for different radar chips.
- r_m is normalized to [-1 1] for convenience.

The cross-correlation between r_o and r_m is computed as:

$$X_{corr}[k] = \sum_{m=-\infty}^{\infty} r_o^*[m] r_m[k + m] \quad (4.2)$$

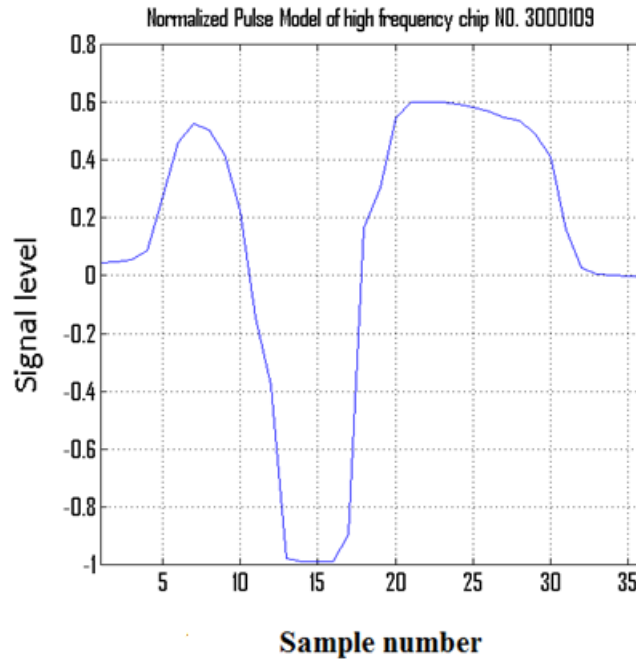


Figure 4.1.: The 'Pulse Model', namely the template of a received pulse signature averaged by 20 measurements from face to face measurements.

where r_o^* is the conjugate of the signal r_o .
Therefore, the position j is found by:

$$\hat{j} = \arg \max_k Xcorr(k) \quad (4.3)$$

where k is the number of the sampling bin and \hat{j} is the estimated index of the window containing the received pulse with maximum likelihood.

The concept of Spatial Domain Signature Matching is quite straight forward. More for the method can be found in [4].

This method has its advantage of simplicity, however not the most efficient and robust way for near field radar application. A method based on Time-Frequency analysis will be introduced to obtain a more robust algorithm.

Short Time Fourier Transform based Signature Matching approach

To match the pulse and the template, consistent information should be provided sufficiently. In other words, certain numbers of coefficients are needed to determine the similarity between the transmitted and received pulse signatures. For an Ultra-wide band signal, it is easier to extract coefficients in frequency domain due to the large

bandwidth. For the same reason, the template of the signature in frequency domain should be also generated from a pulse signature which is generalized enough, namely whose coefficients therefore could represent most cases. A joint time and frequency analysis called 'Short Time Fourier Transform' is applied to characterize the received signal as follows:

$$X(m, \omega) = \sum_{n=-\infty}^{\infty} x(n)w(n-m)e^{-j\omega n} \quad (4.4)$$

where x is the received sequence in time domain, w is a window function, whose shape is to be selected. This basically could be interpreted as a localized Fourier Transform within a sliding window, which slides one by one sample through the whole sequence x . The window size here is chosen to have the same length as the pulse template signature as introduced in previous section. By this approach, both time resolution and frequency resolution could be obtained, not only for pulse locating but also for signature analysis. Wider window size leads to higher frequency resolution, while smaller window size provides higher time resolution. From the uncertainty principle, the best resolution for both couldn't be achieved at the same time. From this point of view, different window shapes will give different results and the optimal choice could be obtained by a Gaussian Window [5].

Note that from an practical point of view, the Fourier transform could be expressed as a multiplication of the signal and an N -point Discrete Fourier Transform (DFT) matrix W .

An N -point DFT is expressed as a matrix multiplication $X = Wx$, where X is the signal after DFT, x is the original input signal in time domain and W is the transformation matrix with size $N \times N$, defined as:

$$W = 1/\sqrt{N} \begin{bmatrix} 1 & 1 & 1 & 1 & \dots & 1 \\ 1 & e^{-j\frac{2\pi}{N}} & e^{-j\frac{4\pi}{N}} & e^{-j\frac{6\pi}{N}} & \dots & e^{-j\frac{2(N-1)\pi}{N}} \\ 1 & e^{-j\frac{4\pi}{N}} & e^{-j\frac{8\pi}{N}} & e^{-j\frac{12\pi}{N}} & \dots & e^{-j\frac{4(N-1)\pi}{N}} \\ 1 & e^{-j\frac{6\pi}{N}} & e^{-j\frac{12\pi}{N}} & e^{-j\frac{18\pi}{N}} & \dots & e^{-j\frac{6(N-1)\pi}{N}} \\ \vdots & \vdots & \vdots & \vdots & \ddots & \vdots \\ 1 & e^{-j\frac{2(N-1)\pi}{N}} & e^{-j\frac{4(N-1)\pi}{N}} & e^{-j\frac{6(N-1)\pi}{N}} & \dots & e^{-j\frac{2(N-1)(N-1)\pi}{N}} \end{bmatrix} \quad (4.5)$$

Thus, without modification, a template matching for Time-frequency analysis will be presented as:

$$Xfcorr(k) = Wr_o(k + 1 : k + N_1) * H(Wr_m) \quad (4.6)$$

where K , $Xfcorr$, R_o and R_m are the sample index, the cross correlation, the received signal and the pulse template respectively, in frequency domain and n_w is the window size.

Here, the sample index with maximum likelihood is defined as following the same rule as in Equation 4.3:

$$\hat{j} = \arg \max_K Xfcorr(K) \quad (4.7)$$

Therefore, STFT provides the coefficients in frequency domain within the sliding window. However, from a robustness viewpoint, not all the coefficients are supposed to be used for this matching algorithm, since in such cases, this algorithm will give an identical result as spatial domain matched filter technique. As stated in Chapter 3, the low frequency component indicates clutters; the signal received over the wireless channel spans a large bandwidth, from 1.5 to 5 GHz in this case, and the coefficients higher than this frequency band could be safely considered as noise. This fact could be seen in Figure 4.2 and Figure 4.3, the spectrum of the pulse template and the spectrum of the received signal within the matched window has a clearly linear relationship. Therefore, a pre-filtering procedure should be carried out before the cross-correlation is computed. The pre-filtering is considered as a coefficient selection problem, which is implemented either by applying a band-pass filter to each STFT sequence, or equivalently a simple modification of the DFT matrix since we only consider filter with rectangular shape:

$$W' = diag(\beta)W \quad (4.8)$$

where β is a coefficient vector whose entry gives weight to each frequency component and $diag(\beta)$ is a diagonal matrix with the coefficients from β as the diagonal entries.

In order to achieve a more stable and robust result, Spatial matched filter and Time-frequency analysis are combined as shown in Figure 4.4. There are several ways to combine the results, and one way is to take the linear combination as follows:

$$\alpha(k) = (aXcorr(k) + bXfcorr(k)) \quad (4.9)$$

where, $k = 1, 2, \dots, n - n_w$.

$$\hat{j} = \arg \max_k \alpha(k) \quad (4.10)$$

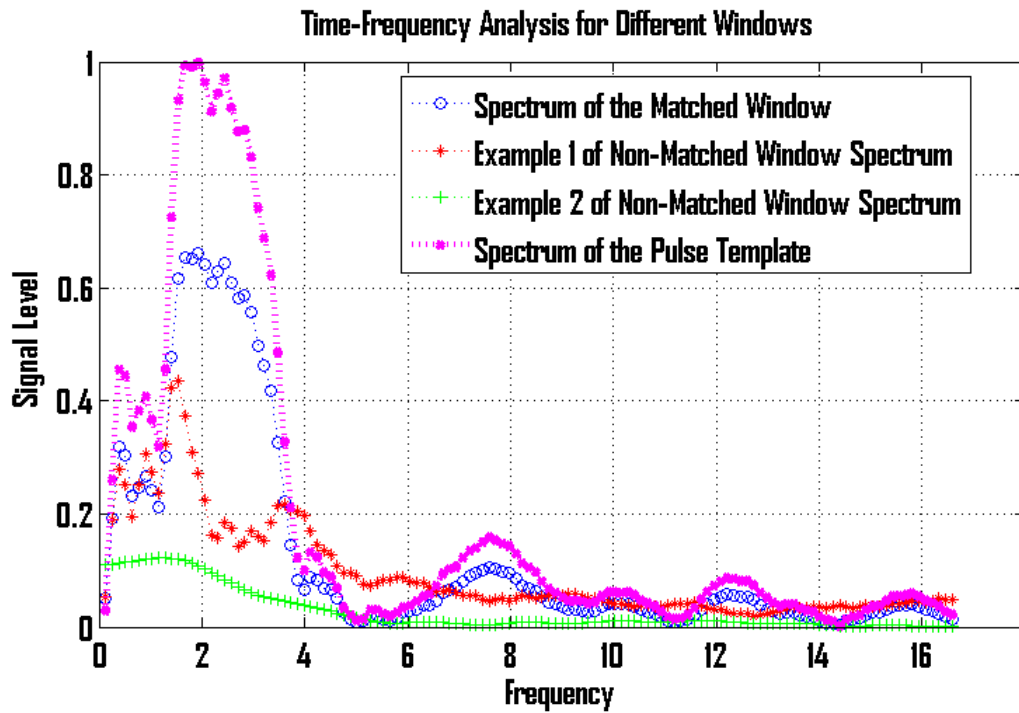


Figure 4.2.: Clutter map evaluation by the value of constant frequency component

where, a and b are chosen in order to get the minimum validation error. After normalization of the cross-correlation result, linear combination is the most stable way to get a robust estimation.

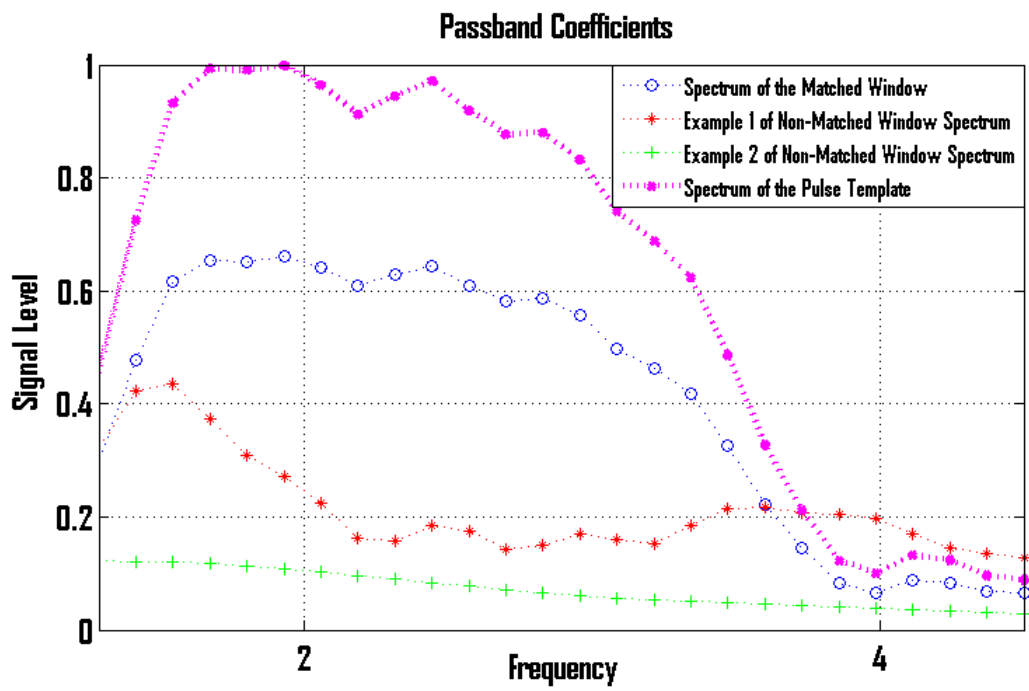


Figure 4.3.: Clutter map evaluation by the value of constant frequency component

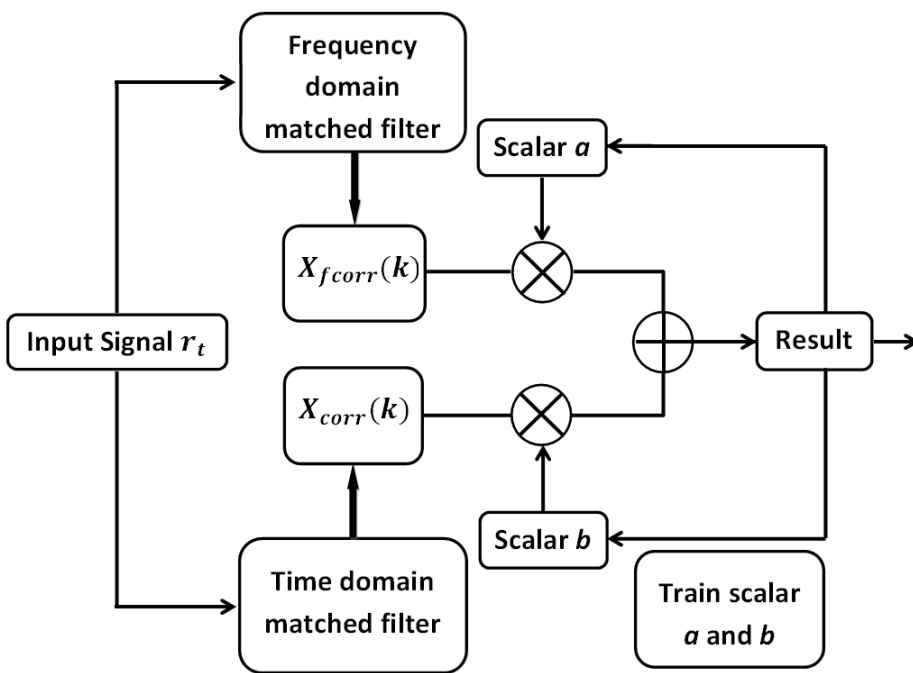


Figure 4.4.: A linear combination result of Spatial Signature Matching and STFT based approach.

Another additional operation is to smooth the combination result before taking the maximum value. This is done by a moving average filter, in order to get rid of the effect from outliers.

'Position Matrix' and Least Square approach

As discussed before, in Spatial Domain Signature Matching section, the estimation of j could be obtained by computing the maximum value in cross-correlation in (4.3). This can be expressed identically as:

$$\hat{j} = \arg \max_k (r_o^T M(:, k)) \quad (4.11)$$

where, r_o is a signal vector with length 128, M is a matrix with size $128 + n_w \times 128$, which is defined as:

$$M = \begin{bmatrix} r_m & 0 & 0 & 0 \cdots & 0 \\ 0 & r_m & 0 & 0 \cdots & 0 \\ \cdots & & & & \\ 0 & 0 & 0 & 0 \cdots & r_m \end{bmatrix} \quad (4.12)$$

where r_m is a column vector with length n_w and M is called 'Position Matrix', since it spans all the possible positions in signal vector r_o .

Now we consider a least square based approach, which is represented as follows:

$$\hat{\alpha} = \arg \min_{\alpha} (\|M\alpha - r_o\|_2^2) \quad (4.13)$$

where α is a column vector with length 128; each entry of α is a scalar indicating the likelihood of the corresponding pulse position, from 1 to 128; then j is determined by:

$$\hat{j} = \arg \max_k (|\hat{\alpha}(k)|). \quad (4.14)$$

The idea here is that after re-scaling each column of position matrix M by the corresponding element in α , the difference between the received signal and the summation of all the possible positions in this re-scaled position matrix is minimized. By comparing this similarity between the received signal and all the possible positions, the 'non-similar' positions are suppressed that only the 'true position' will stand out.

However, in practice, a L-2 norm minimization gives a dense result in α , which increases false alarm rate.

To remove this effect, instead of taking the maximum value of α , we integrate α over a sliding window with size $2n_k$, where n_k is estimated practically. Therefore, the pulse indication is defined as:

$$\hat{j} = \arg \max_k (S_{\alpha(k)}) \quad (4.15)$$

where,

$$S_{\alpha(k)} = \begin{cases} \sum_{l=1}^k \frac{\alpha(l)}{k} & \text{when } k \leq n_k \\ \sum_{l=k-n_k}^{k+n_k} \frac{\alpha(l)}{2n_k} & \text{when } k > n_k \end{cases} \quad (4.16)$$

is the 'averaged' integration of α .

The advantage of this approach is that it is more robust and with low complexity. Since the Position Matrix M is a full rank and sparse matrix, the estimation for α can be computed directly by the matrix operation:

$$\hat{\alpha} = (X^T X)^{-1} X^T r_o \quad (4.17)$$

Weighted Least Square based approach

In Time-Frequency analysis, as we emphasized previously, features from the spectrum are easy to extract due to the large bandwidth. Moreover, to either locate or analyze the pulse signature, we have to select the most characteristic frequency coefficients with respect to some certain objectives. Obviously, the coefficients within the bandwidth draws more attention, since the high frequency components indicate noise, and the low frequency component represent the clutters. Thus this problem could be somehow presented as a weighted problem, since our attention is not uniformly distributed over the whole spectrum.

The main idea of this matching approach along with a brief proof is shown below.

First, a window of size n_w slides over all the samples in r , and at each sample, the window is called 'window k ' which starts from the k^{th} sample of r . So we have:

$$\hat{\alpha}(k) = \arg \min_{\alpha} (\|r_m - \alpha(k)r(k : k + n_w)\|_2^2) \quad (4.18)$$

where $k = 1, 2, \dots, 128 - n_w$ and α is a vector with length $128 - n$.

Then the best match is found by:

$$\hat{j} = \arg \min_k (\|r_m - \hat{\alpha}(k)r(k : k + n_w)\|_2^2) \quad (4.19)$$

which could also be described as the size of the vector obtained by projecting the measured signal onto the space spanned by the orthogonal complement to the r_m signal, where the projection matrix is defined as:

$$P(k) = I - \frac{r(k : k + n_w)r(k : k + n_w)^T}{r(k : k + n_w)^T r(k : k + n_w)} \quad (4.20)$$

and therefore,

$$\hat{j} = \arg \min_k (\|P(k)r_m\|_2^2) \quad (4.21)$$

In either way, transformed to frequency domain, the expression of the criteria has not been changed. A brief proof is as follows:

- In least-squares form:

In frequency domain, it could be written as:

$$\hat{j} = \arg \min_k (\|R_m - \hat{\alpha}(k)R(k : k + n_w)\|_2^2) \quad (4.22)$$

since we have:

$$\sum_{k=1}^{128-n_w} e_k = \sum_{K=1}^{n_w} E_K \quad (4.23)$$

where e is the squared error vector we have computed as above, and E is the corresponding frequency expression (as we said before, DFT matrix W is an unitary matrix and thus preserves L2 norm). Here, k and K are the indexes of the samples in the time domain and frequency domain respectively. To simplify, we only use k to indicate the sample numbers in later formulation.

This means \hat{j} indicates the best match for the pulse location in the received sequence both in time and frequency domain.

- In projection matrix form:

Since Discrete Fourier Transform (DFT) is an unitary transformation, the projection matrix in frequency domain is:

$$P_f(k) = I - \frac{Wr(k : k + n_w)(Wr(k : k + n_w))^H}{(Wr(k : k + n_w))^H Wr(k : k + n_w)} \quad (4.24)$$

Thus,

$$P_f(k) = I - \frac{Wr(k : k + n_w)(Wr(k : k + n_w))^H}{r(k : k + n_w)^H r(k : k + n_w)} \quad (4.25)$$

since unitary transformation does not change inner product. It could be further re-written as:

$$\begin{aligned} P_f(k) &= I - \frac{Wr(k : k + n_w)r(k : k + n_w)^T W^H}{r(k : k + n_w)^T r(k : k + n_w)} \\ &= WW^H - \frac{Wr(k : k + n_w)r(k : k + n_w)^T W^H}{r(k : k + n_w)^T r(k : k + n_w)} \\ &= WP(k)W^H \end{aligned} \quad (4.26)$$

and

$$(WP(k)W^H)(Wr) = W(P(k)r) \quad (4.27)$$

So that \hat{j} could be estimated as:

$$\hat{j} = \arg \min_k |W(P(k)r(k : k + n_w))| \quad (4.28)$$

will give the same result as in time domain.

Now let's come back to frequency domain least square interpretation. If we give weights to the errors, we have:

$$E_{weighted} = \sum_k^{n_w} w_{kk} E_k \quad (4.29)$$

where the weights are chosen to minimize the errors within the passband of the signal in both time domain and the frequency domain.

Weight selection: First, the relationship between the pulse template R_m and the received signal $R(k : k + n_w)$ (in the frequency domain) is analyzed. If we plot the samples of R_m and $R(k : k + n_w)$ as y and x axis respectively in Figure 4.5, we will get a cloud around the $\hat{a}(k)R(k : k + n_w) + b$ which is shown as the red straight line, and b is the constant bias. To minimize the overall error, the samples need to be weighted. The reason is that some of the samples in $R(k : k + n_w)$ do not play equally important roles as the others in this matching problem.

There are several ways to achieve this goal; the technique employed here is to use a Neural Network [6] for this weight optimization problem. In this case, as we can see in figure 4.6, a network structure with one layer (no hidden layer), $n_w + 1$ -dimensional

input and 1 dimension output has been used. The input vector contains the squared errors E_K obtained from the previous section; the output is one single neuron whose value is either one (match!) or zero (not match!). The optimal weight vector is obtained by back propagation.

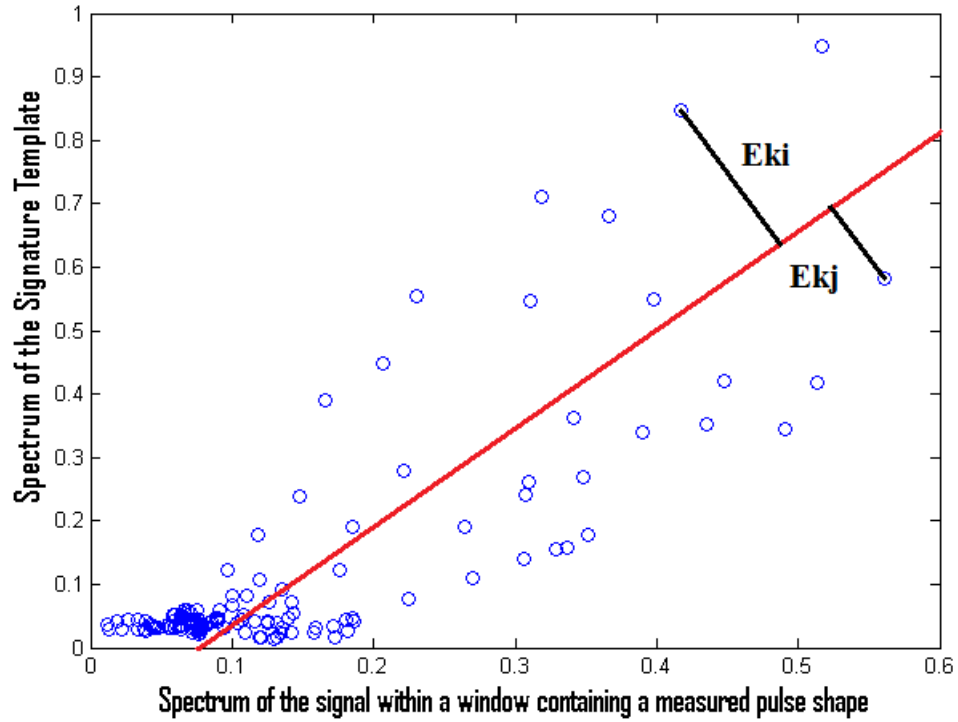


Figure 4.5.: Relation between the spectrum of the Signature Template and the measured signal spectrum.

ANN model:

- Objective: classify the part of the received signal within a sliding window as either containing or not containing a reflected pulse from the target of interest;
- Input ζ : $n_w + 1$ dimensional squared error vector;
- Output O : one dimension with value 1(containing the pulse) or 0(not containing the pulse);

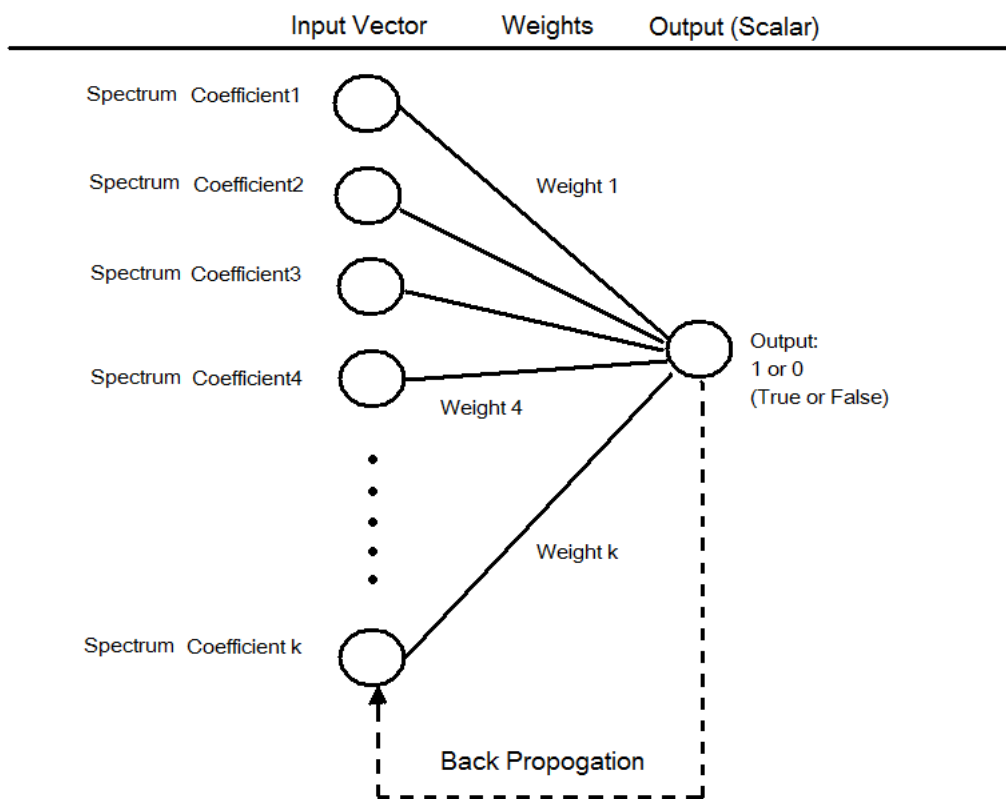


Figure 4.6.: Basic structure of the Neural Network

- Training set: a set of training data with known input and known output ζ ;
- Optimization procedure:
 - Normalize the input vectors to $[-1 \ 1]$.
 - Initialize the weights randomly between $[-1 \ 1]$.
 - Iteration:
 - * for $i = 1 : \text{size of the training set}$
 - Compute error $\zeta - O$
 - Compute δ_o for all weights from input layer to output layer
 - Update the weights
 - * end

Advantages: The advantage for a neural network in this case is as follows.

- It is natural for weights optimization;
- The training data is easy to obtain;
- It is a visualized model whose structure could be easily changed;

A one layer feed forward architecture has been used for now since we need a robust result in order to cover all the cases. The structure could be further optimized by other techniques whereas we will not go into details. Therefore, in principle, the meaning of the result here is that if the input $\zeta(k_1)$ does not have significant effects on the output O , the weight for that particular input $w(i)$ will be small; on the other hand if the input $\zeta(k_2)$ plays a crucial role for the classification result, the weight will be relatively large.

Convexity and neural network:

The entries of this N dimensional weight vector are corresponding to the essentiality of the n_w frequency coefficients. From our prior knowledge of the system, this significance is according to the signal spectrum, which is shown in Figure 4.7. As we can see, in the frequency domain, the 3 dB Bandwidth is roughly from 1.8GHz to 3.9GHz. Regarding the passband, there are also some patterns between 3.9GHz to 10GHz with some variation, the local maximum at frequency 7.8GHz, for instance.

These patterns might be different for each particular system, but is identical to some extent for all measurements from the same system. Loosely speaking, the more 'important' coefficients in frequency domain will be the ones within the system bandwidth. However, even within the bandwidth, at some frequencies, the radiation power has been split due to the nature of the antenna. Therefore, the significant coefficients will be considered roughly as 1.5Hz - 4Hz, 6.5Hz - 9Hz, which are supposed to be strongly correlated with the training result of the neural network.

The result analysis can be found in following sections.

L1 norm minimization

As stated before, L-2 norm minimization will result in a dense α whereas what we need is a sparse result. Thus instead of L2-norm minimization, we use L1 minimization which gives the sparsest result [8].

First, we can model the matching problem as a L0-norm optimization:

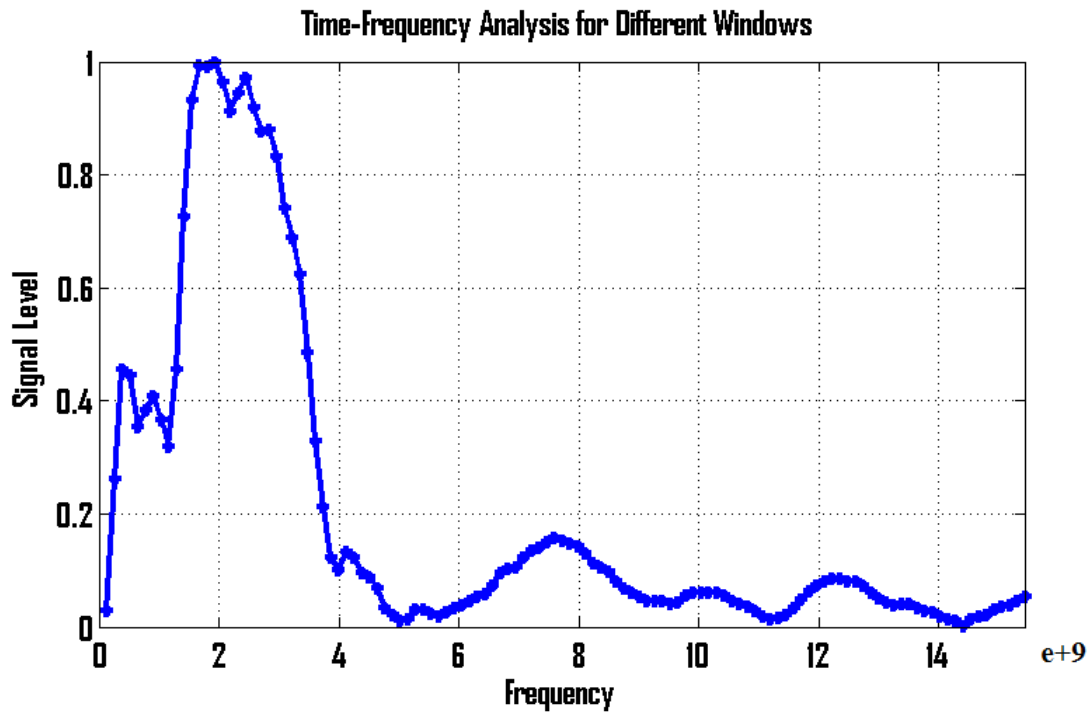


Figure 4.7.: This figure shows the patterns in the spectrum of the reflected signal.

$$\begin{aligned} \min_{\alpha} \quad & \|\alpha\|_0 \\ \text{subject to} \quad & M\alpha = r \end{aligned} \quad (4.30)$$

where M is the position matrix; and $\|\alpha\|_0$ is the L0-norm of the vector α , namely the number of its non-zero coefficients. In this case, $\|\alpha\|_0$ indicates the number of the objects.

This optimization problem is proved to be equivalent as a L1-norm optimization:

$$\begin{aligned} \min_{\alpha} \quad & \|\alpha\|_1 \\ \text{subject to} \quad & M\alpha = r \end{aligned} \quad (4.31)$$

which can be solved in different ways. The solution in this project is obtained by recasting the problem as a linear programming problem.

Multiple-object locating and tracking will be discussed in later sections.

4.2.2. Sub-sample resolution and differential ranging

Since all above discussed pulse locating approaches are sample based, the best achievable locating resolution is the sample resolution which in this case is 4.5 mm. In order to have better locating resolution than the sampling resolution, the fractional sample shift has to be determined. One straightforward way is to do interpolation between two measured samples. But this method has its own drawbacks: firstly, more samples will cause longer processing time; secondly, limited resolution results from finite interpolation; thirdly, inaccurate estimation for interpolation leads to less accurate results. Here, we use a Fourier transform based technique to obtain a sub-sample resolution. The theory is given here and the measurement result will be shown in later sections.

Suppose we have two signals. They are identical but with a slight time delay. The time delay can be determined by the division of the Fourier transform.

Fourier Transform based differential phase

We have two signals $s_1(t)$ and $s_2(t)$:

$$s_2(t) = s_1(t - \tau) \quad (4.32)$$

The Fourier transform of the signals is as follows:

$$S_1(\omega) = S_2(\omega)e^{-j\omega\tau} \quad (4.33)$$

If s_1 and s_2 are identical signals with a phase shift, they will have the following relation in the frequency domain:

$$\frac{S_2(\omega)}{S_1(\omega)} = e^{-j\omega\tau} \quad (4.34)$$

Therefore, the angle will be a linear relation:

$$\angle \frac{S_2(\omega)}{S_1(\omega)} = -\omega\tau \quad (4.35)$$

The time shift τ can then be determined.

In practice, after obtaining the sample based pulse location \hat{j} , we form a reference signal by placing the signal model on sample \hat{j} and apply this Fourier transform based approach in order to get a subsample resolution.

4.2.3. Multi-target Locating

In the previous sections, we have discussed about ranging for only one target within the view of the radar. This is very useful since in most cases we only consider the closest target; or we process the targets separately with an antenna array, where each radar chip is only responsible for the processing of one target. Nevertheless, we also developed multi-object detection algorithm to handle the case that multiple targets are observed in the view of one radar. The same technique for one target ranging can also be applied in multi-object scenario. The only extra processing is to identify multi-maxima in α which is computed by any method introduced in the Section 4.2.1. The number of maxima indicates the number of observed objects.

First, we smooth the coefficients in α by 5-points moving average as follows:

$$\alpha(k) = \sum_{i=k-2}^{i=k+2} \frac{\alpha(i)}{5} \quad (4.36)$$

Then we estimate the maximum points by a simple and fast algorithm which simultaneously identifies the maxima by the tendency (intends to increase or decrease) of the curve around each point. If the curve first goes up and then decreases, we assume that there is steady point and thus a maximum occurs correspondingly.

Another way to locate multiple targets is to use L1-norm minimization introduced previously, and the peaks in the sparse result give the possible locations of the targets.

4.2.4. Calibration

The estimation of the pulse location is in the unit of samples. In applications, ranging requires a distance based result. Here we need a calibration procedure to obtain the conversion between number of samples and actual range. The equation is as follows:

$$d = \frac{\Delta_{s1}j_1 + \Delta_{s2}j_2}{2} \quad (4.37)$$

where d is the range of the target; Δ_{s1} is the sample interval when the pulse travels in the air and Δ_{s2} represents the sample interval in the cables; j_1 and j_2 are the corresponding sample number at which the target locates.

As analyzed in Chapter 1, $\Delta_{s2}j_2$ has a approximately fixed value c and j_1 is a variable as a function of temperature and humidity.

We can re-write the equation as:

$$d = \frac{\Delta_{s1}j_1 + c}{2} \quad (4.38)$$

where Δ_{s1} represents the spatial distance between two consecutive samples; j_1 is the corresponding numbers of samples the pulse is located; and c is the constant value of the cable length which could be written as $\Delta_{s2}j_2$ in this context.

Therefore, to obtain the range d , we shall determine the value of $\Delta_{s1}j_1$ and $\Delta_{s2}j_2$ in the following way:

A known object is placed at two known ranges d_1^1 and d_1^2 away from the radar system. For each measurement, we have:

$$\hat{j}^1 = j_1^1 + j_2 \quad (4.39a)$$

$$\hat{j}^2 = j_1^2 + j_2 \quad (4.39b)$$

where d^i is the range of the object plus the length of the cable; \hat{j}^i is the estimated pulse location in sample unit, and j_2 is the constant.

Also, at the same temperature, we have:

$$d^1 = \frac{\Delta_{s1}j_1^1 + c^1}{2} \quad (4.40a)$$

$$d^2 = \frac{\Delta_{s1}j_1^2 + c^2}{2} \quad (4.40b)$$

Therefore,

$$\hat{\Delta}_{s1} = \frac{2d^1 - 2d^2}{\hat{j}^1 - \hat{j}^2} \quad (4.41)$$

and so j_1^i can be computed as:

$$\hat{j}_1^i = \frac{2d^i - c^i}{\hat{\Delta}_{s1}} \quad (4.42)$$

So we have:

$$\hat{j}_2 = \hat{j}^i - \hat{j}_1^i \quad (4.43)$$

Therefore, for each new measurement, we have:

$$\hat{j}_1 = \hat{j} - \hat{j}_2 \quad (4.44)$$

and

$$\hat{d}_1^i = \frac{\Delta_{s1}(\hat{j}^i - \hat{j}_2^i)}{2} \quad (4.45)$$

where only Δ_{s1} remains unknown for a different environment condition. Therefore, we need at least one instant training measurement under the same condition to determine the uncertainty.

Furthermore, the CMOS UWB chip is not temperature stable, which means the transmitted pulse signature varies with temperature [2]. Therefore, the calibration is very crucial for each measurement in a temperature changing environment. In order to develop a simple, efficient and accurate calibration method, we have investigated the following.

Direct Coupling Calibration

The way here is to utilize the direct coupling between the two antennas.

As we have introduced in the Chapter 1, direct coupling might be a disturbing part for ranging. However, since the distance between the two antennas is fixed, and the direct coupling is the first part to be received (assume that the antennas are close enough), instead of gating it out, we could use it to calibrate the system. Before any new measurement, the system will automatically measure the location of the direct coupling, with respect of number of samples, which is assumed to be within the sample range 50 to 150. According to the radar equation, the propagation time is half of the reflection time.

For a new measurement, from the derivation above, we have the distance between the two antennas written as:

$$d_{ant} = \Delta_{s1}(\hat{j} - \hat{j}_2) \quad (4.46)$$

Since the d_{ant} is a known parameter, we can compute the variable Δ_{s1} instantly under the certain environment condition as:

$$\hat{\Delta}_{s1} = \frac{d_{ant}}{\hat{j} - \hat{j}_2} \quad (4.47)$$

Note that by using this calibration method, the condition is that the target should be at least placed at twice of the range between the parallel antennas. Namely:

$$d_{min} = 2d_{ant} \quad (4.48)$$

Where d_{ant} is the distance between the two antennas, d_{min} is the minimum range from the antenna to the target and the d_{max} is defined by the dynamic range of the radar system.

4.3. Method and Evaluation

4.3.1. Evaluation of the pulse locating approaches

System calibration

First, the system calibration is carried out and evaluated by the accuracy of ranging result. To have a fair comparison, ranging with and without calibration are both based on manual observation. The sample at which the object is located depends on the first peak of the received pulse. Without calibration, we assume that $\Delta_{s1} = 0.45mm$. So we have the estimation:

$$\hat{d} = 0.45(\hat{j} - \hat{j}_2) \quad (4.49)$$

The results are shown in Figure 4.8. As we can see, without calibration, the system has a larger deviation.

Ranging

We have tested the 5 different pulse locating techniques for a set of 40 measurements. The object we use is a metal ball with a 200 millimeter diameter. The measurement is carried out in an anechoic chamber. The true position of the object is measured by a measuring tape with 3 meters length in total with 1 millimeter resolution. The distance between the two antennas is 250 mm. All the 5 approaches are applied after clutter removal as discussed in Chapter 3.

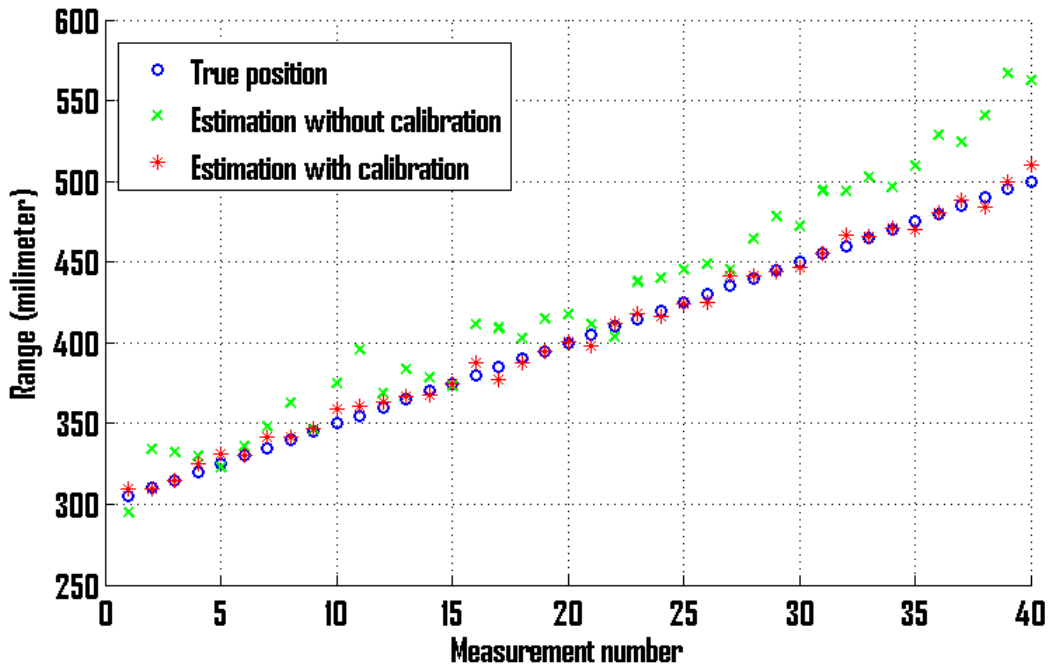


Figure 4.8.: The evaluation of the system calibration. As shown in this figure, the estimation without the calibration of the system gives a larger deviation from the true positions.

The comparison result is shown in Figure 4.9 and the RMSE for each result is presented in Table 4.1.

The advantage of STFT based approach is that it is a fast method since it only involves some linear transformation (STFT) and computation for cross correlation. Also, it works even in the presence of clutter because of the pre-filtering procedure that allows it to get rid of the relatively constant reflection which is considered as the clutter. The same result is observed for WLS based approach since the weight selection helps the algorithm to ignore the low frequency component in the received signal. This could be seen in Figure 4.10. The PMLS based technique is also with low complexity as discussed in Section 4.1.1.

For WLS based approach, we compared the results for different weight selection methods which includes ANN-based weight optimization and manual weight selection. It turns out that weight selection plays an important role for ranging. As we can see in Figure 4.11, the ANN-based weight optimization gives a better result.

Table 4.1.: Comparison of the target locating techniques in terms of RMSE.

Algorithm	RMSE
Spatial matched filter	9.2187
STFT based matched filter	2.6659
PMLS	2.2216
Weighted least square	1.8476
L1-norm minimization	1.9085
Phase-correlation	2.7986
Phase-correlation + STFT technique	1.1037

When the parameter Averaging Factor decreases, the processing will be faster but the noise level is higher. To test the robustness of the algorithms, we add a Gaussian White Noise to the received signal. The standard deviation increases from 0.2 to 1. The SNR is defined as:

$$SNR = \frac{A}{\sigma} \quad (4.50)$$

where $A = 0.6125$ is the mean of the received raw signal and σ is the standard deviation of the artificial noise.

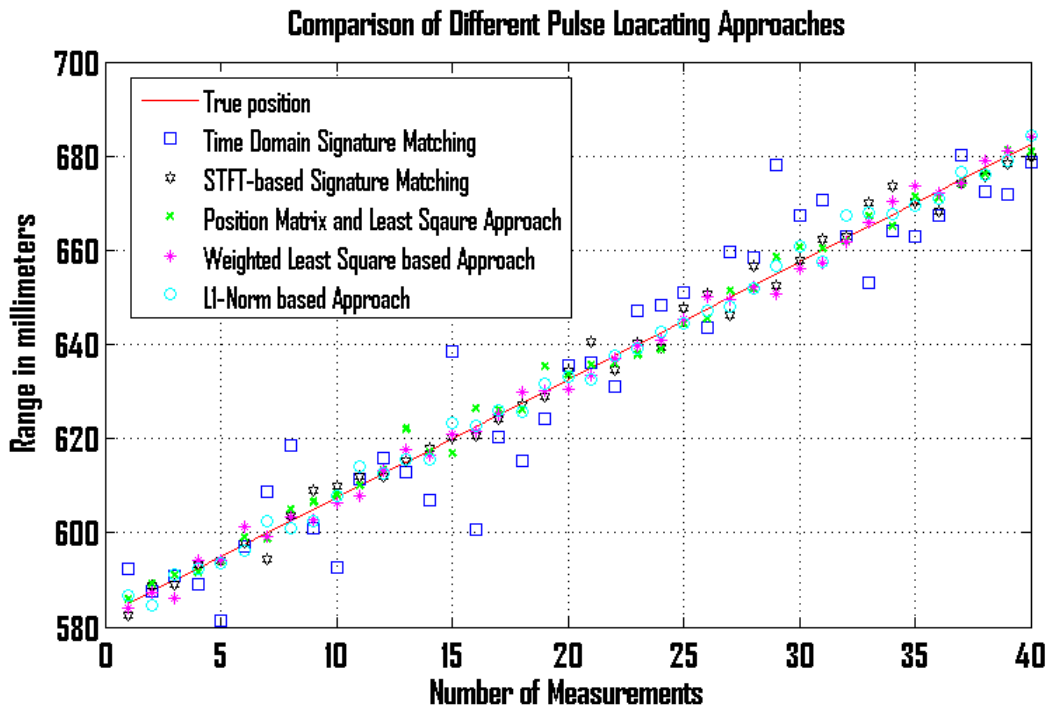


Figure 4.9.: Comparison of the 5 different pulse locating approaches in terms of the Root Mean Square Error (RMSE). The RMSE are shown in Table 4.1. The pulse locating techniques are carried out after clutter removal. As we can see, except the Spatial Domain Signature Matching technique, the other methods obtain similar results.

First we estimate and remove the clutter, and then apply the pulse locating algorithms. We compare the STFT and PMLS based approaches in Figure 4.13 and the result shows that the later gives a good accuracy even with extremely low SNR as shown in Figure 4.12.

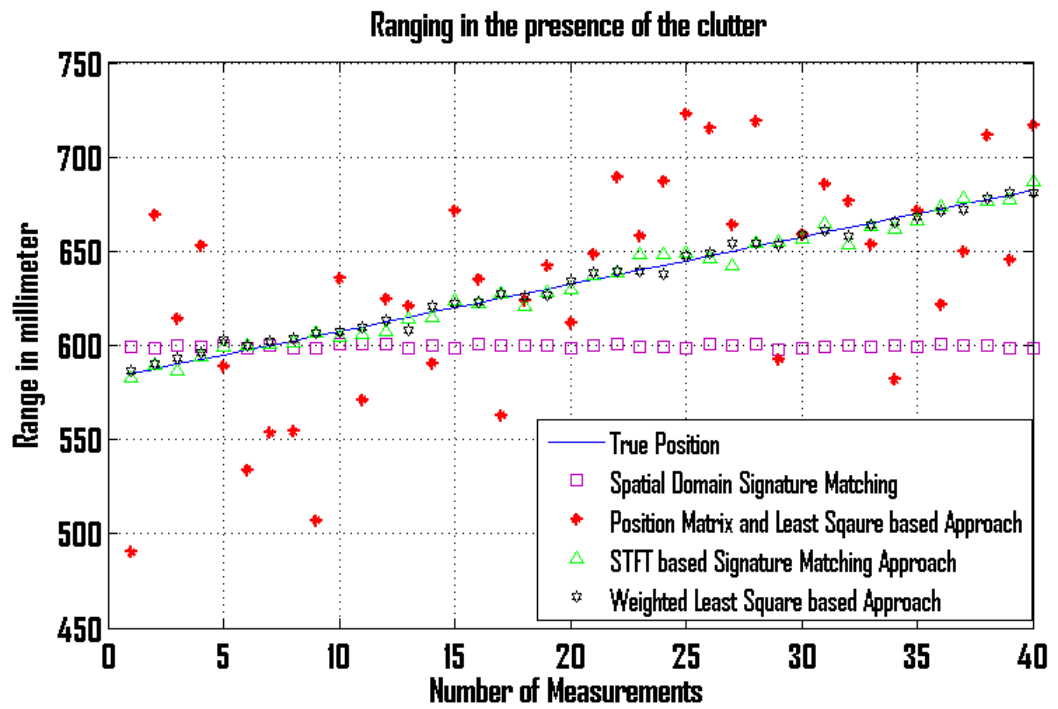


Figure 4.10.: Pulse locating results in the presence of clutter. The STFT and WLS based approaches both give good results where the result of WLS is slightly better than the other.

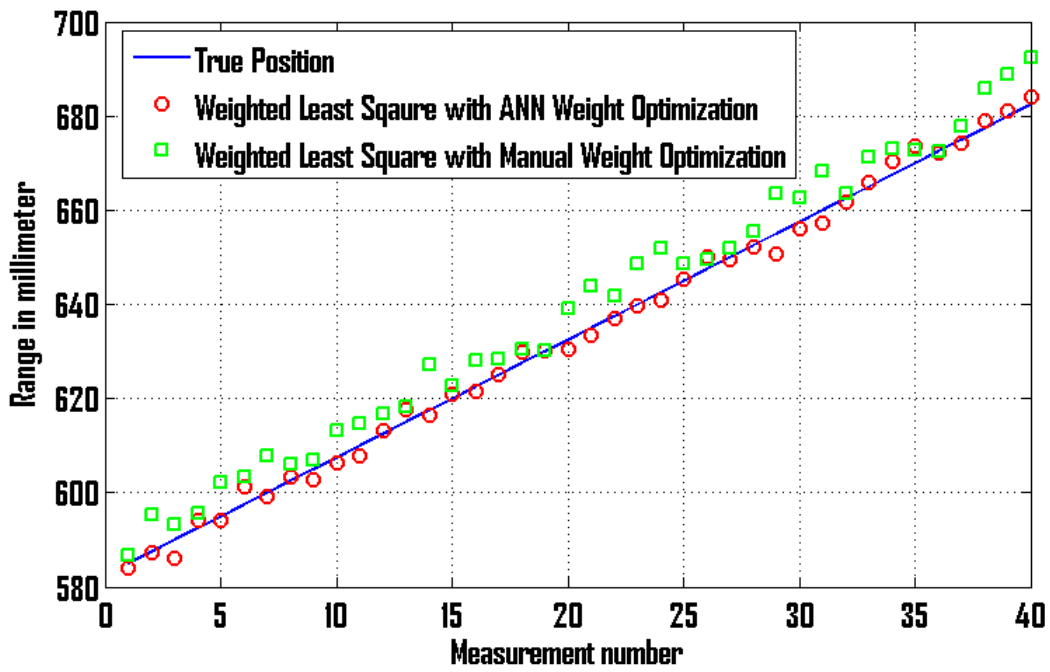


Figure 4.11.: Different weight selection methods effect the result of ranging to some extent. The ANN-based approach gives a better precision.

Pulse locating in an extremely noisy scenario by Position Matrix and Least Square based Approach

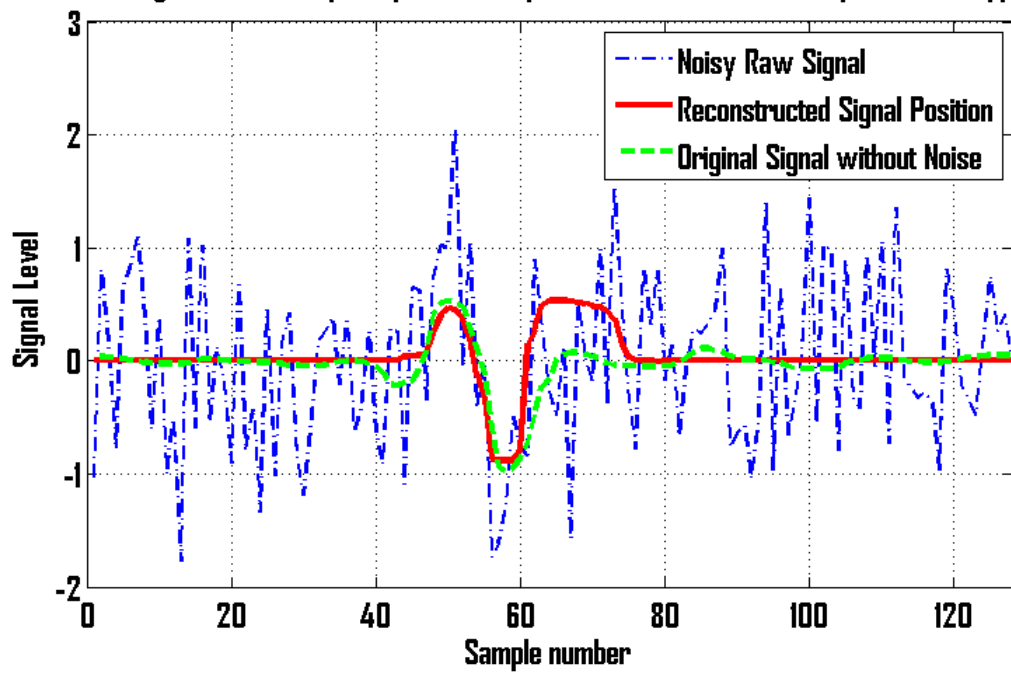


Figure 4.12.: Pulse locating by PMLS based approach with extremely low SNR.

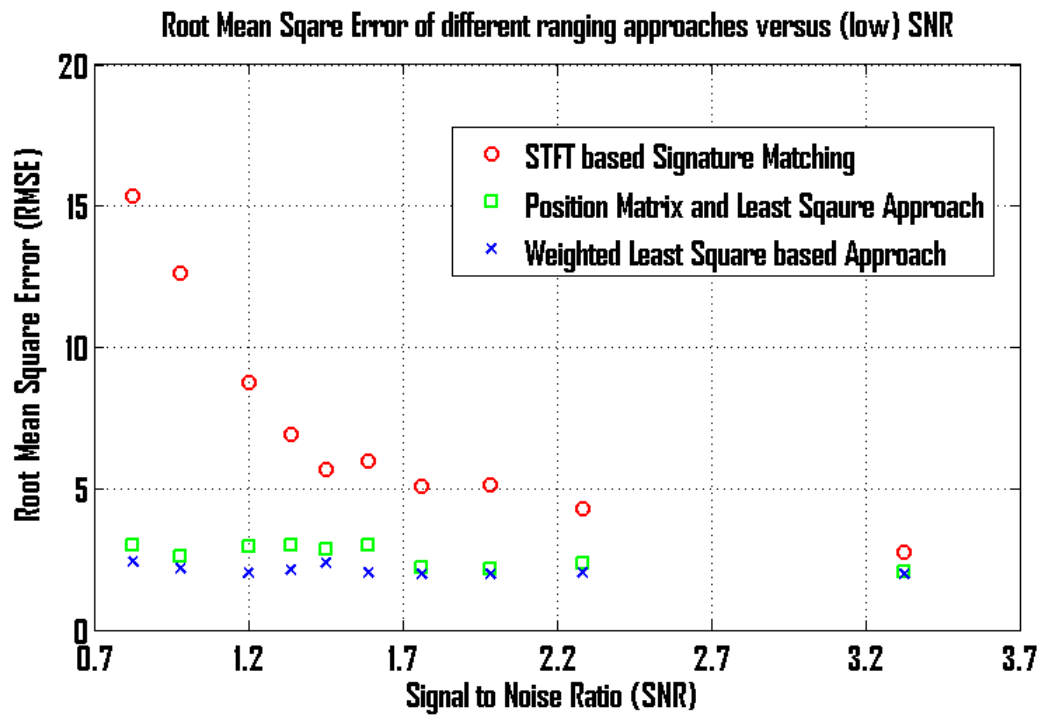


Figure 4.13.: Results comparison between STFT and PMLS based approaches. With low SNR, PMLS gives a much better precision than STFT.

Results for sub-sample resolution is shown in Figure 4.16. A 1 mm resolution is obtained by this approach. An example of phase correlation is shown in Figure 4.14 and 4.15, where 4.14 shows the relative positions of the pulse shape and the pulse template and 4.15 shows the phase correlation function of the two signals.

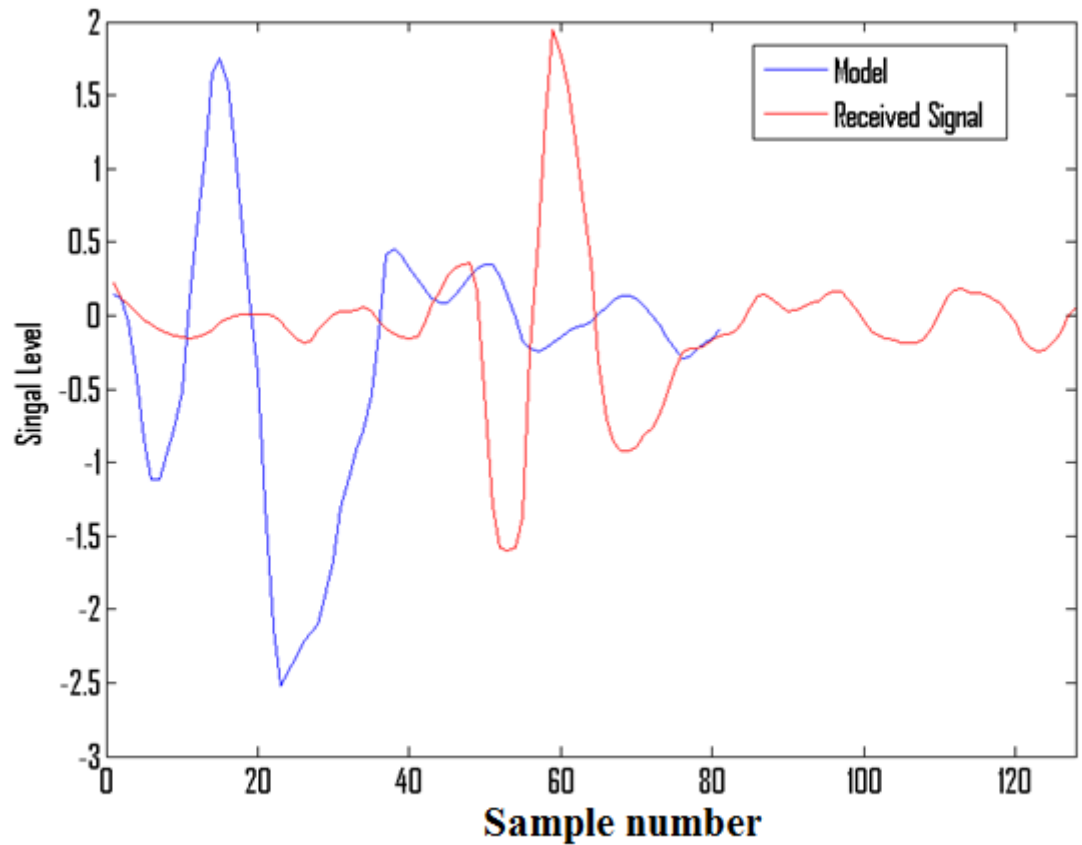


Figure 4.14.: The received signal and the signal template which is placed manually at the first sample.

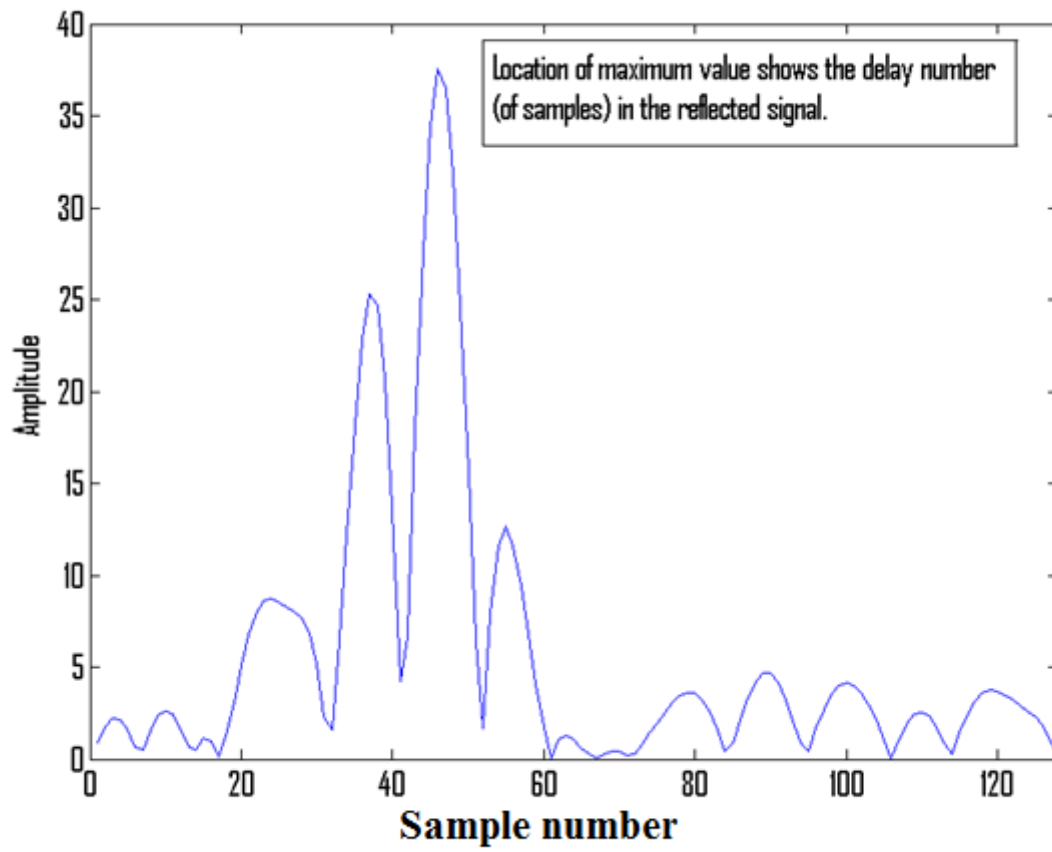


Figure 4.15.: Phase correlation function between the two signals.

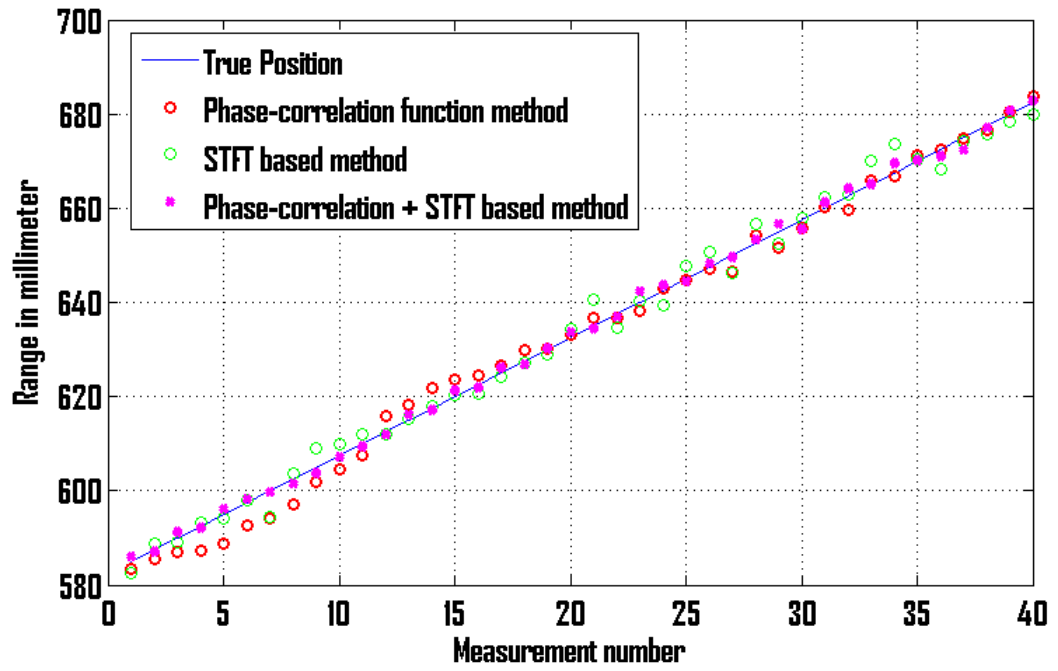


Figure 4.16.: Ranging with sub-sample resolution determined by phase correlation.

4.4. Conclusion

In this chapter, we discussed about ranging by different techniques. The techniques are evaluated in different scenarios and compared both theoretically and practically. It turns out that the STFT based method provides the best trade-off between complexity and estimation accuracy. Sub-sample resolution is achieved by phase correlation function and can be used in differential ranging applications. The calibration procedure updates the pulse model r_m and the conversion equation between number of samples and distance in millimeter unit.

5. Tracking

In this Chapter, with pulse locating techniques stated previously, Kalman filter [9] based tracking algorithm is presented. First, we will discuss Kalman filter in this particular application; then, the algorithm will be extended to two dimensional case; finally, a multiple object tracking is implemented.

5.1. Theory

Tracking requires fast and reliable measurements in real time. Based on the conclusion from Chapter 4 that the STFT based pulse locating technique is a good trade-off between the complexity and accuracy, it has been applied in this case for the tracking algorithm.

5.1.1. Kalman filter for one dimensional tracking

For one dimensional tracking, only the range to the antenna is measured in real time. A Kalman filter is applied in this case to estimate the position and velocity of the object. After pulse locating, the measurement z is known and adaptively corrected in real time by Kalman filter update.

Initialization

- State x is formed by position and velocity:

$$x_k = [p, \dot{p}]^T \quad (5.1)$$

where p indicates the target position.

- Observation is given by measured position: z_k .
- Initial state covariance matrix:

$$\mathbf{P}_{0|0} = \begin{bmatrix} A & 0 \\ 0 & B \end{bmatrix} \quad (5.2)$$

where A and B are chosen practically as 3 and 1 respectively.

- Observation noise v_k :

v_k is assumed to be zero mean Gaussian white noise with covariance R_k .

$$\mathbf{v}_k \sim N(0, \mathbf{R}_k) \quad (5.3)$$

- Process noise w_k :

w_k is assumed to be zero mean Gaussian white noise with covariance Q_k .

$$\mathbf{w}_k \sim N(0, \mathbf{Q}_k) \quad (5.4)$$

- Step size and transfer matrix:

Transfer function F with step size T is given by:

$$F = \begin{bmatrix} 1 & T \\ 0 & 1 \end{bmatrix} \quad (5.5)$$

T is selected to be unit time.

- Observation matrix C :

C represents the relation between the true state x_k and measurement z_k . Here since the transform is just a matter of noise, C is initialized as:

$$C = \begin{bmatrix} 1 & 0 \end{bmatrix} \quad (5.6)$$

Kalman equation

Kalman update for this application is summarized as follows:

- Prediction of error covariance:

$$\mathbf{P}_{k|k-1} = \mathbf{F}\mathbf{P}_{k-1|k-1}\mathbf{F}^T + \mathbf{Q}_k \quad (5.7)$$

- Compute innovation covariance:

$$\mathbf{S}_k = \mathbf{C}\mathbf{P}_{k|k-1}\mathbf{C}^T + \mathbf{R}_k \quad (5.8)$$

- Kalman's gain:

$$\mathbf{K}_k = \mathbf{P}_{k|k-1}\mathbf{C}^T\mathbf{S}_k^{-1} \quad (5.9)$$

- Prediction of state estimation:

$$\mathbf{x}_{k|k} = \mathbf{F}\mathbf{x}_{k|k-1} \quad (5.10)$$

- Prediction of observation:

$$\mathbf{z}_{k|k-1} = \mathbf{C}\mathbf{x}_{k|k-1} \quad (5.11)$$

- State estimation update:

$$\hat{\mathbf{x}}_{k|k} = \hat{\mathbf{x}}_{k|k-1} + \mathbf{K}_k(\mathbf{z}_k - \mathbf{z}_{k|k-1}) \quad (5.12)$$

- Error covariance update:

$$\mathbf{P}_{k|k} = (\mathbf{I} - \mathbf{K}_k\mathbf{C})\mathbf{P}_{k|k-1} \quad (5.13)$$

The result is evaluated in later sections.

5.1.2. Two dimensional tracking

When the tracking is extended to two dimensional, there are several issues to be taken into account.

Radar scope

Radar scope, or the scope of two dimensional measurement, is decided by system property; namely, the dynamic range of the system and the radiation pattern of the antenna.

Setup

To locate an object in two dimensions, there are two ways to set up the antennas: orthogonal and parallel.

- Orthogonal setup:

In this case, we have two pairs of antennas orthogonal to each other as printed in Figure 5.1. The coordinates are computed as follows:

$$d^2 = d_1^2 + d_2^2 \quad (5.14a)$$

$$\alpha_1 = \arccos\left(\frac{d^2 + r_1^2 - r_2^2}{2dr_1}\right) \quad (5.14b)$$

$$\beta_1 = \arccos\left(\frac{d_1}{d}\right) \quad (5.14c)$$

$$\gamma_1 = \alpha_1 + \beta_1 \quad (5.14d)$$

$$\alpha_2 = \arccos\left(\frac{d^2 + r_2^2 - r_1^2}{2dr_2}\right) \quad (5.14e)$$

$$\beta_2 = \arccos\left(\frac{d_2}{d}\right) \quad (5.14f)$$

$$\gamma_2 = \alpha_2 + \beta_2 \quad (5.14g)$$

$$y = d_1 - r_1 \cos(\gamma) \quad (5.14h)$$

$$x = d_2 - r_2 \cos(\gamma) \quad (5.14i)$$

where, the notations are labeled in Figure 5.1. The x and y are the position of the target on x - and y - axis respectively.

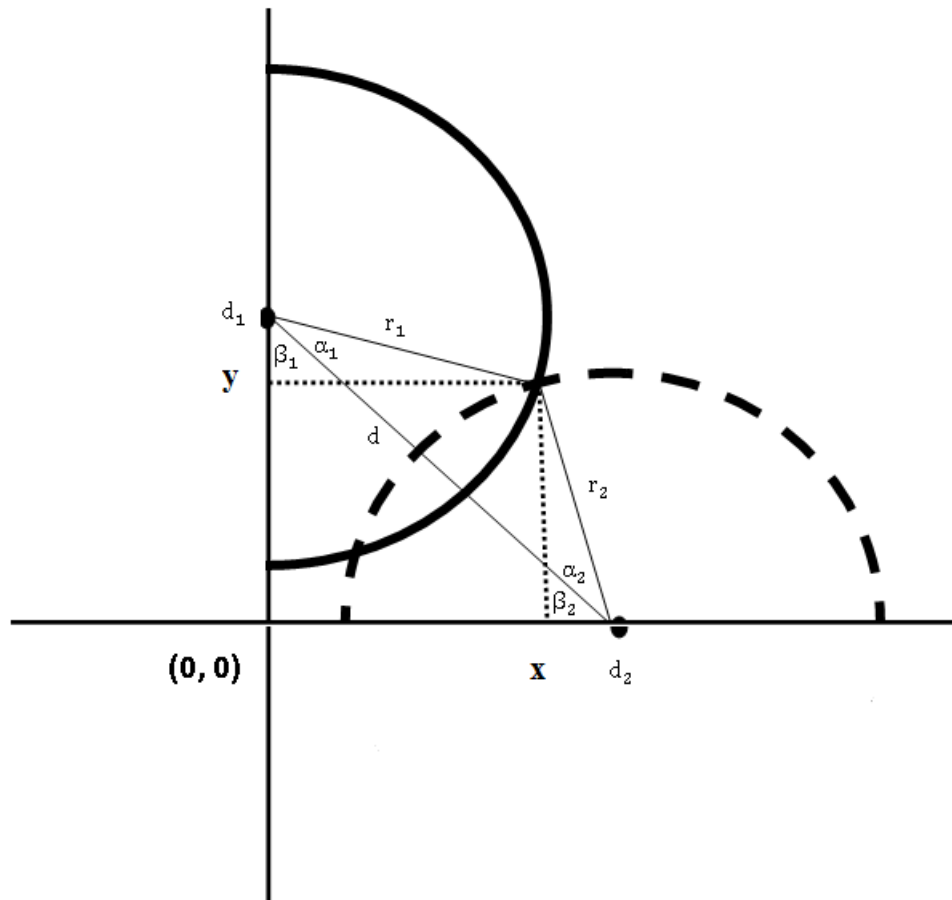


Figure 5.1.: The orthogonal setup of the two radar system for the 2 dimensional tracking. The circle is the radius of the measurement. The center of the circle is the position of the antenna.

– Parallel setup:

As we can see, there will be always ambiguity in orthogonal setup, because of the multiple intersection between the 2 measurements. Also, the dynamic range is limited according to the position of the antennas. Therefore, a parallel setup is presented to compensate for the drawbacks of orthogonal setup, and is more suitable for some applications that orthogonal antennas are not applicable.

As we can see in Figure 5.2, the two pairs of antennas, or antenna array, are positioned in a parallel manner (shown as the center of the circle, which is the radius of the measurement). Therefore, the two dimensional coordinates are computed as follows:

$$d = d_2 - d_1 \quad (5.15a)$$

$$\beta = \arccos\left(\frac{d^2 + r_1^2 - r_2^2}{2dr_1}\right) \quad (5.15b)$$

$$y = r_2 \sin(\beta) \quad (5.15c)$$

$$\alpha = \arcsin\left(\frac{y}{r_1}\right) \quad (5.15d)$$

$$x = d_1 + r_1 \cos(\alpha) \quad (5.15e)$$

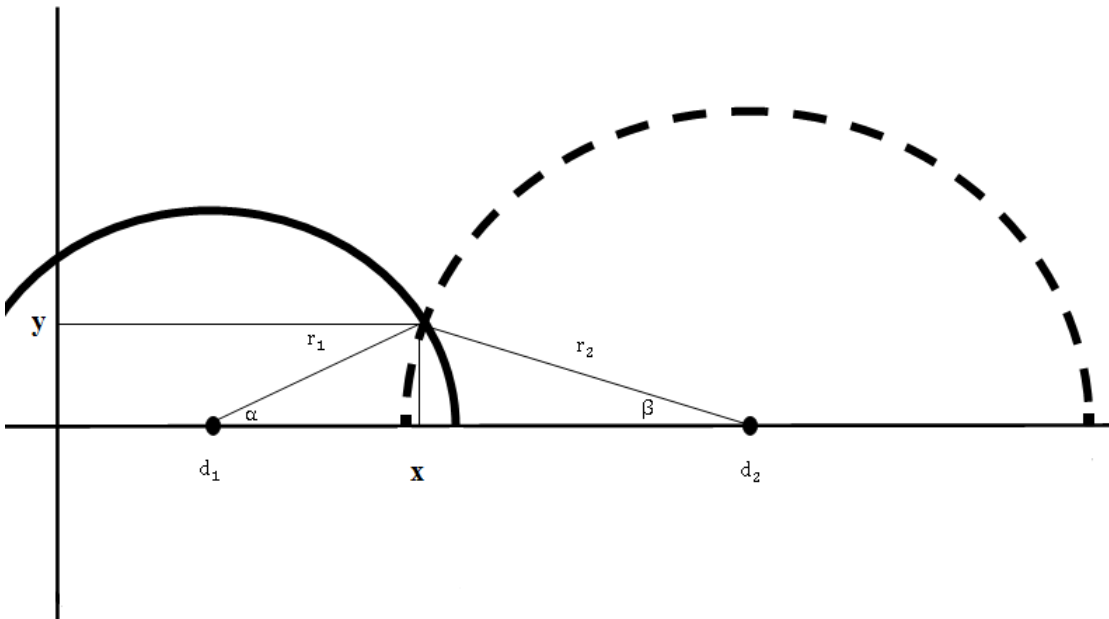


Figure 5.2.: The parallel setup of the two radar system for the 2 dimensional tracking.

Kalman filter for 2D tracking

To extend the Kalman filter to two dimensional case, the observation and state vector are defined as:

$$x_k = [p_x, \dot{p}_x, p_y, \dot{p}_y]^T \quad (5.16a)$$

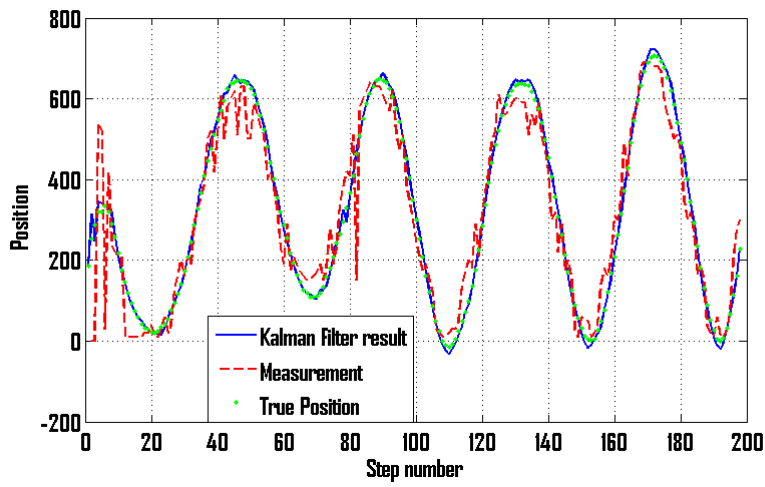
$$z_k = [zx_k, zy_k]^T \quad (5.16b)$$

where zx and zy are the measurement for x and y respectively, which is computed as above. More detail about Kalman filter equation and update could be found in appendix.

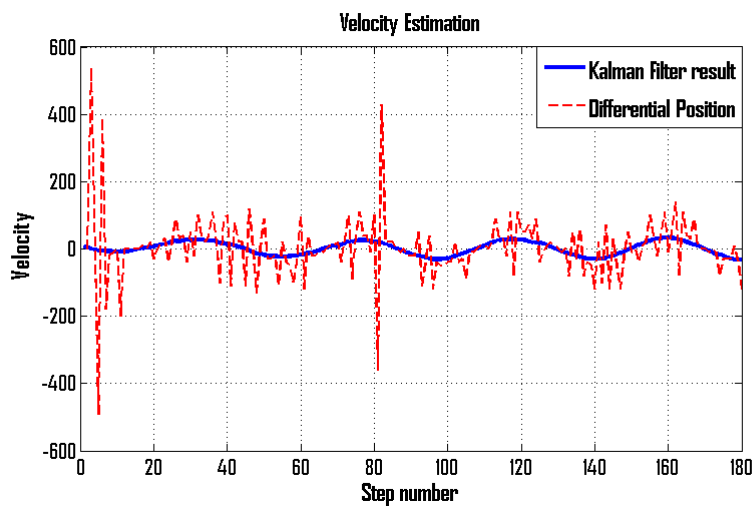
5.2. Evaluation and results

The 1-Dimensional tracking result is shown in Figure 5.3 (a) and (b) for position estimation and velocity estimation respectively. Some inaccurate measurement results are observed in Figure Figure 5.3 (a). One of the main functions of the Kalman filter is to smooth out these outliers to improve the precision. The object is placed in different positions by hand. These true positions are determined by a millimeter resolution scale. The corresponding measured signals are saved for off line evaluation. The algorithms are evaluated in this way: the measured signals are fed into the functions as input; then the estimated positions are as output of the function to compare with the true position. Furthermore, we can estimate the velocity of the moving target by a two-state Kalman Filter which is shown as the blue line in Figure 5.3 (b). The red curve indicates the differential position which is to compare with the estimation result.

Similar results can be observed for two dimensional tracking in Figure 5.4 and 5.5.

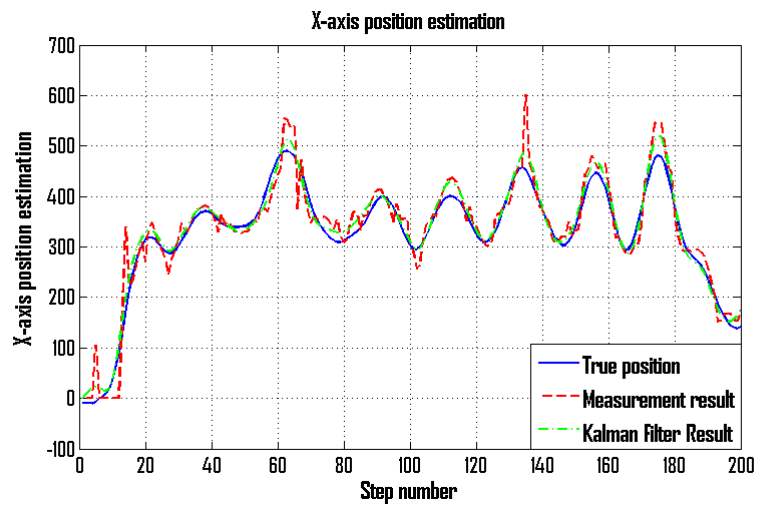


(a) Position Estimation

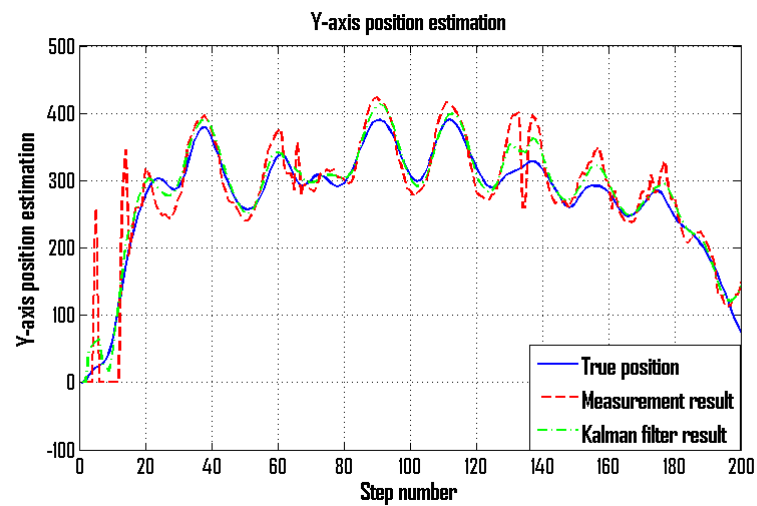


(b) Velocity Estimation

Figure 5.3.: Position (a) and velocity (b) estimation for 1-Dimensional tracking. To compare with, the red curve is shown as the measurement by STFT based Signature Matching. Outliers are observed in the result. The two-state Kalman Filter smoothed out the outliers and estimated the velocity accordingly.

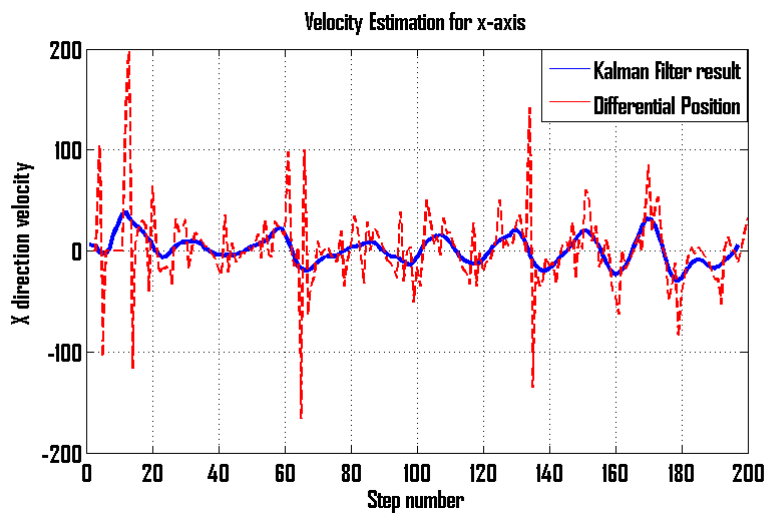


(a) Position Estimation for X-axis

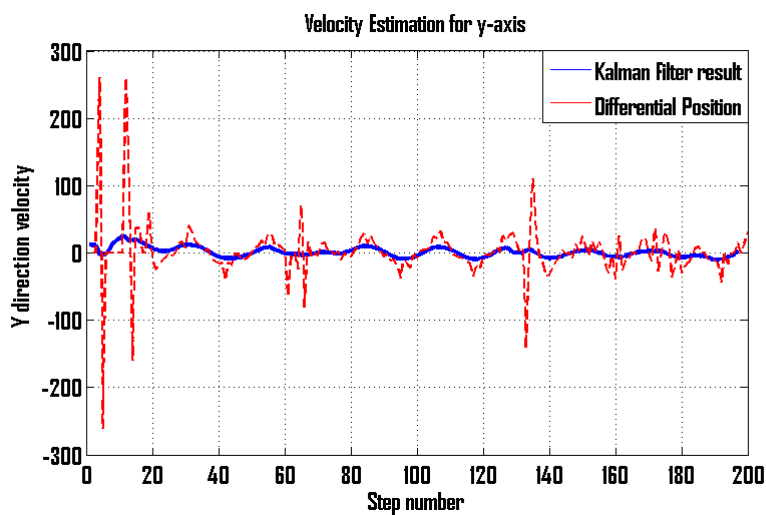


(b) Position Estimation for Y-axis

Figure 5.4.: Position estimation for 2-Dimensional tracking. The red curve in (a) and (b) indicates the measurement by STFT based Signature Matching for X and Y axis respectively.



(a) Velocity Estimation for X-axixs



(b) Velocity Estimation for Y-axixs

Figure 5.5.: Velocity estimation for 2-Dimensional tracking. The red lines whose data are computed from the differential positions of X and Y directions respectively represent the measurement of the velocity; while the blue curves present the estimation from Kalman Filter.

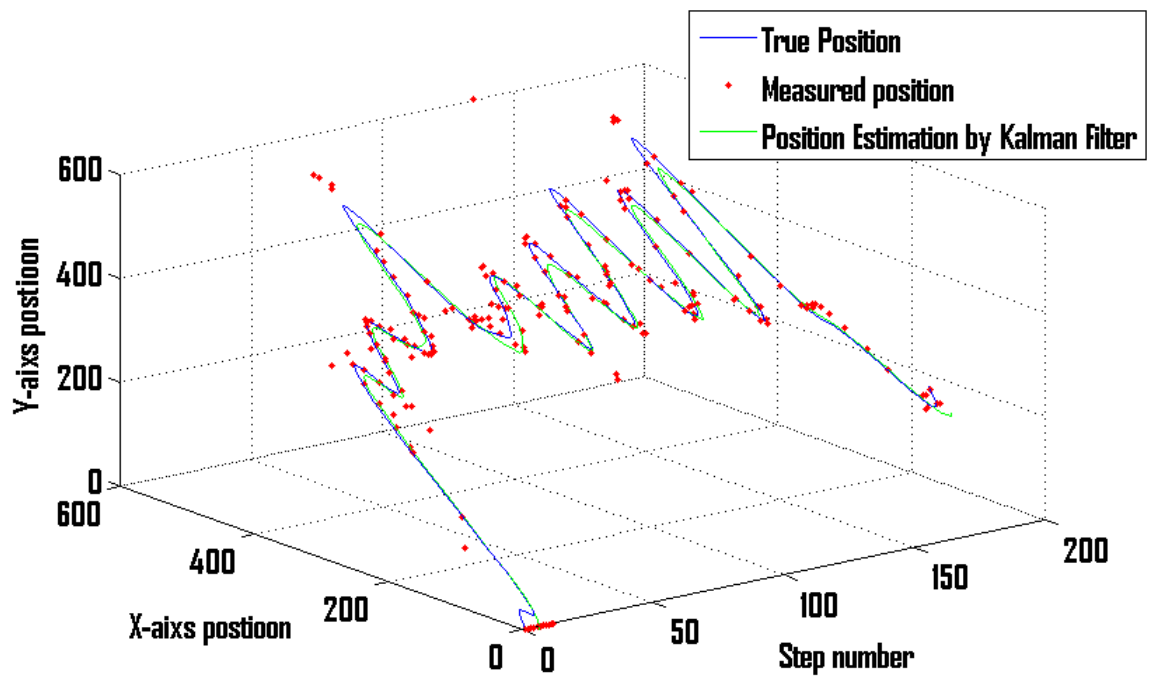


Figure 5.6.: The coordinates for X- and Y-axis as a function of time are plotted in this figure.

5.3. Conclusion

In this chapter, tracking algorithms have been implemented and evaluated. For two dimensional ranging, there are two different setups according to different application requirements. The STFT based approach discussed in Chapter 4 is applied as the real time pulse locating technique in this chapter. Kalman filter is used in both one and two dimensional cases and good results have been achieved.

6. Examples and Demonstration

The user interface is implemented by MATLAB. The interface windows for different functions are shown separately in the following sections.

6.1. Set parameter

Before any operation, the parameters should be set up. The important parameters in this demonstration are shown in Figure 6.2 and the explanations and default values are also listed in 1.1 in Chapter 1.

Among these parameters, the most important ones are 'Frame Offset', 'Averaging Factor' and 'Gain'. Frame Offset (FO) indicates the internal time delay which decides the range of the measurement. For example, $FO = 300$ means the internal time delay is $299 \times 27.8 = 8.312$ ns, which is approximately 1345.5 mm. That means in one measurement, the system will measure the signal reflected between the range of 1345.5 mm and 1895.5 mm. The Averaging Factor (AF) is the number of measurements the system takes and pre-processes internally before the output. AF effects the noise level and the processing speed. When AF is large, the noise level is lower and the processing is slower. The Gain of the transmitted signal determines the transmitted signal level.

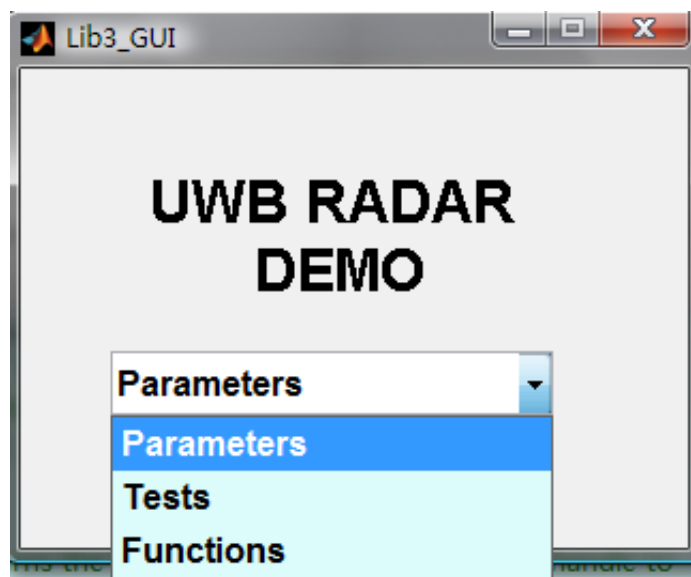


Figure 6.1.: User interface: the main menu

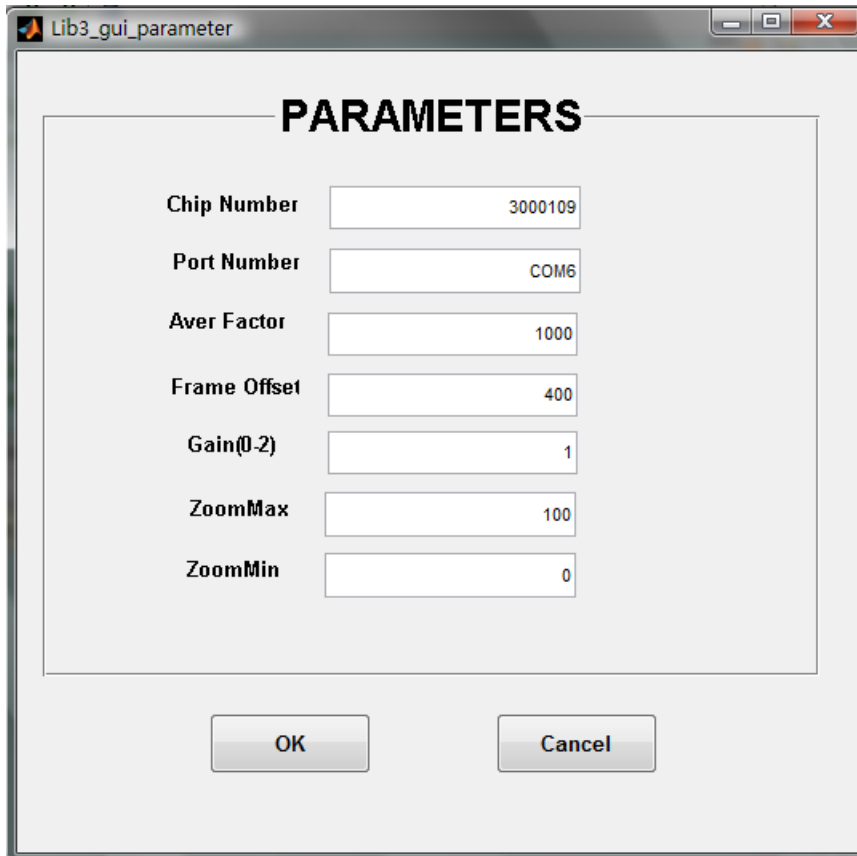


Figure 6.2.: User interface: parameter set up, including the Chip number, the Name of port, the Averaging Factor, the Frame Offset, the signal Gain and the signal Zoommin/Zoommax. The default values are shown in the interface.

6.2. Tests

After setting up the parameters, the 'test' is ready to start. The interface is shown in Figure 6.3.

6.2.1. Raw data

Raw data shows the received signal without any processing in real time. According to the signal model from Chapter 2, this signal is a summation of the clutters, the noise and the reflection from the target. An example is shown in Figure 6.4.

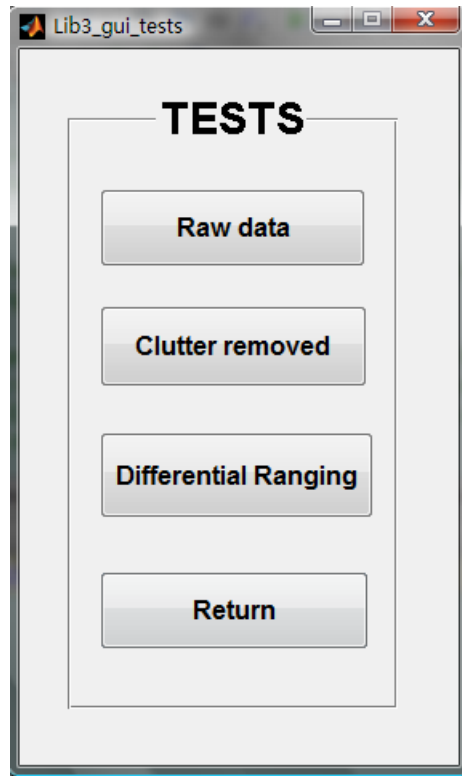


Figure 6.3.: User interface: tests

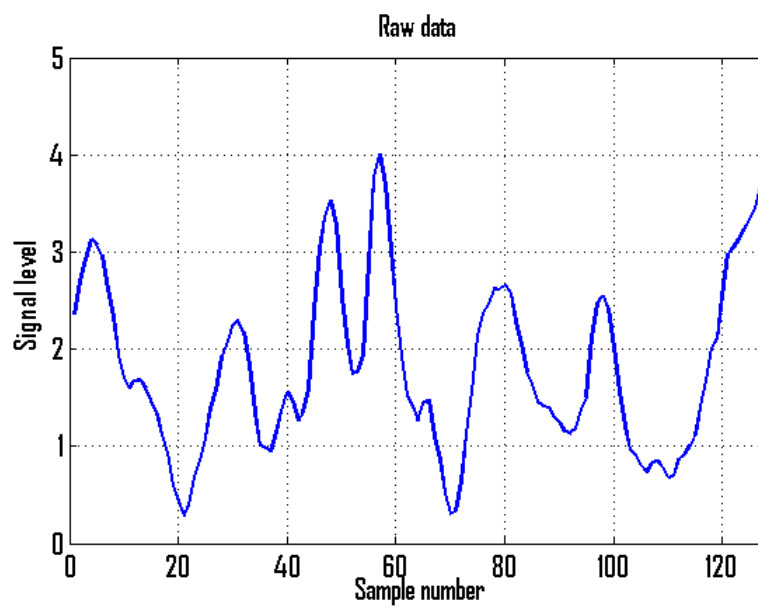


Figure 6.4.: User interface: an example of raw data

6.2.2. Differential ranging

According to the interest of a regular differential movement like heart beat, this demonstration shows the ability of differential ranging with 1 mm resolution. The key here is the phase correlation function as discussed in Chapter 4. The time delay between the two measurements is 0.5 sec in this case. It is shown in Figure 6.5 that the signal after clutter rejection is plotted in real time and the differential range is displayed on the title of the figure accordingly.

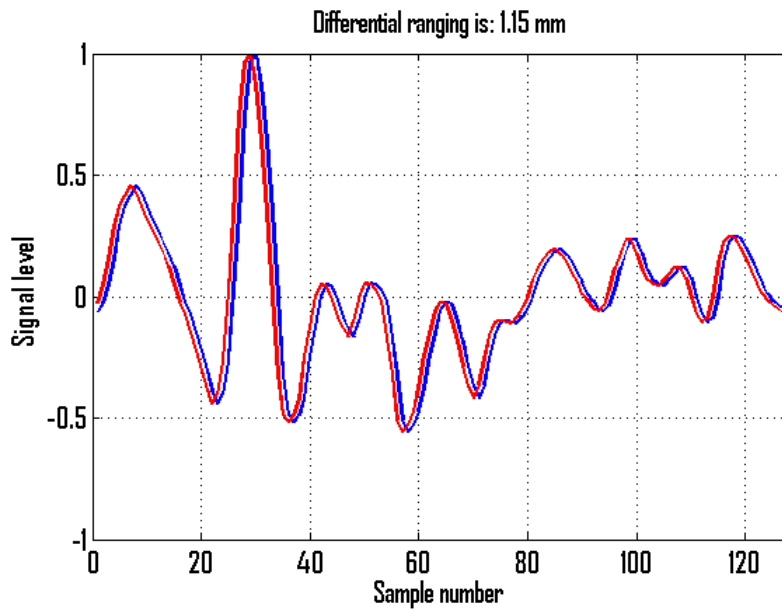


Figure 6.5.: User interface: an example of differential ranging. The blue and red curves indicate identical signals with a slight time shift.

6.3. Functions

The interface of the 'Functions' is shown in Figure 6.6.

6.3.1. Calibration

Before starting any demonstration in the function menu, we need to calibrate the system by clicking on the 'Calibration' button. The formula for ranging and the pulse template will then be updated. The calibration is done by the direct coupling between the two antennas.

6.3.2. Clutter estimation

After calibration, another important procedure is clutter map estimation. The theory and the results are discussed in Chapter 3. This clutter map generation is a necessary procedure for ranging, but not for tracking since it is an adaptive clutter removal technique.

6.3.3. Ranging

Ranging with one target

As discussed in Chapter 4, there are five alternative approaches to choose, and each of them has its own advantages and drawbacks. After choosing one preferred method, the range will be displayed on the user interface in a millimeter unit.

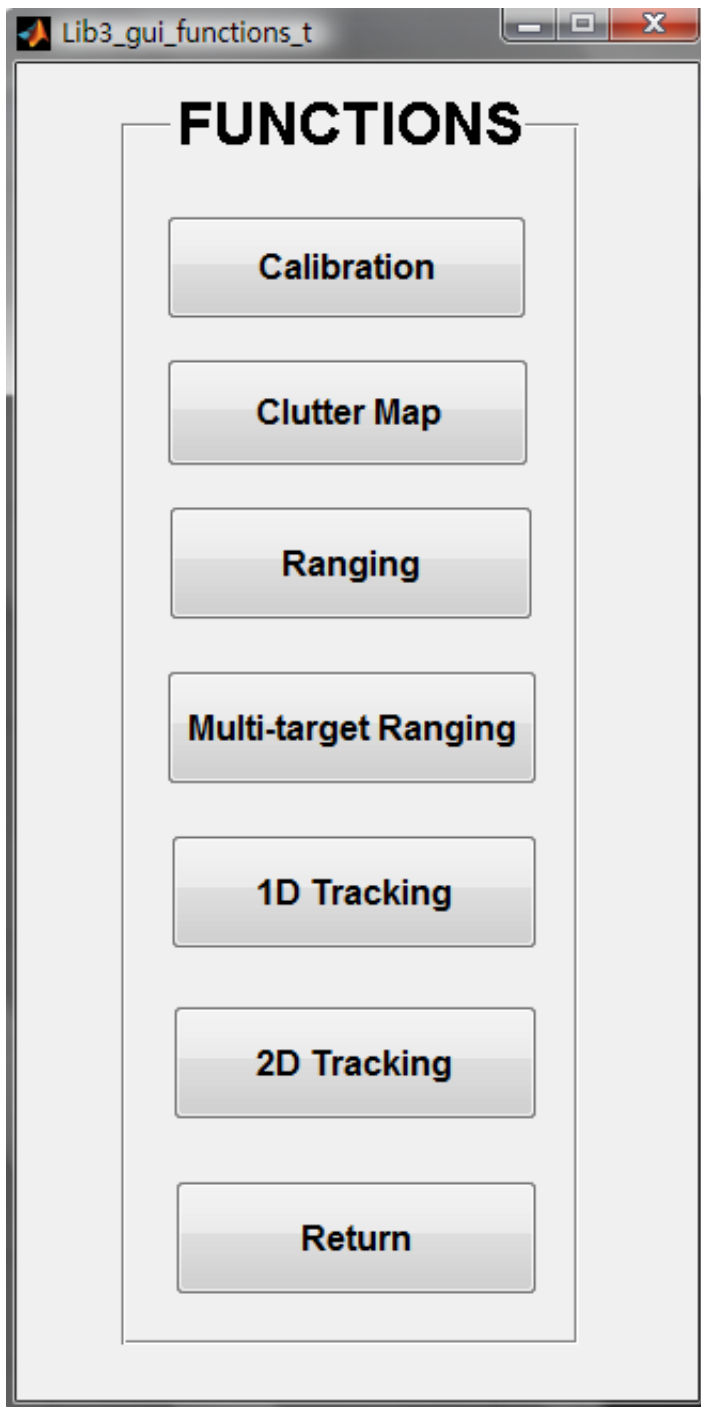


Figure 6.6.: User interface: the functions

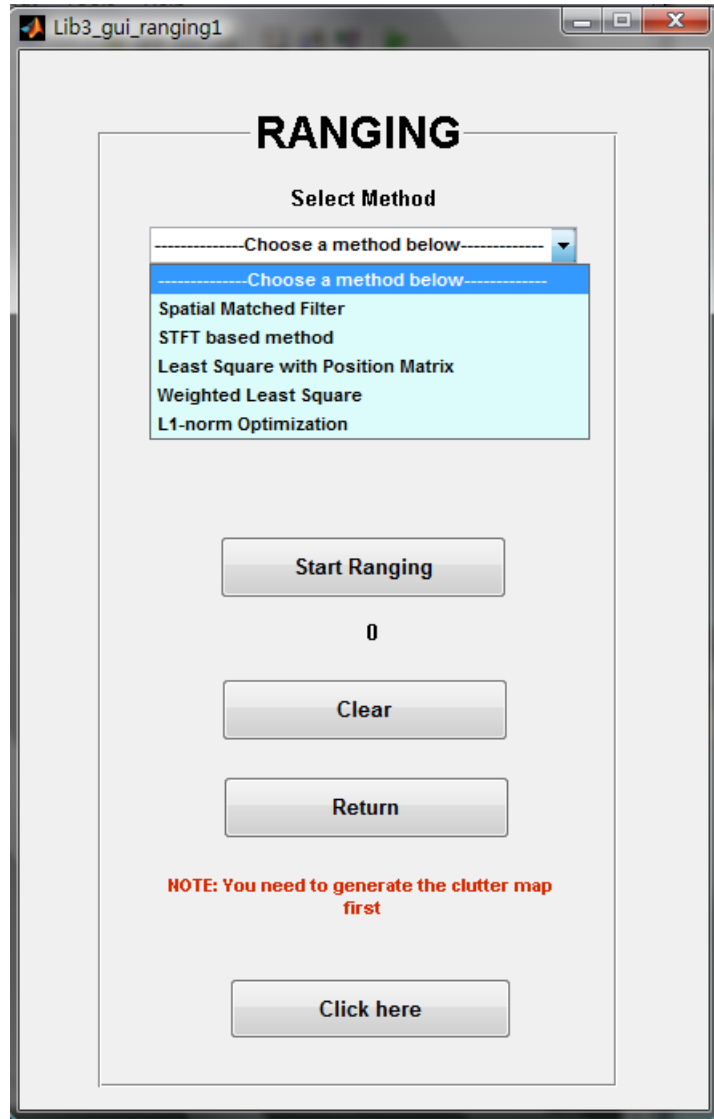


Figure 6.7.: User interface: ranging

Multiple target ranging

The interface for multiple target ranging is the same as for one target, while the best choice for multi-target ranging method is PMLS or L1-norm.

The result is shown in Figure 6.8. In this case, there are two target in the view of the radar. The green windows indicate the locations of the pulses in terms of number of samples. The conversion between 'number of samples' and 'distance in millimeters' has been introduced in Chapter 4, Calibration section. The range is determined by the starting edge of the window. The technique used here was PMLS. The result in millimeter unit is displayed in the GUI window.

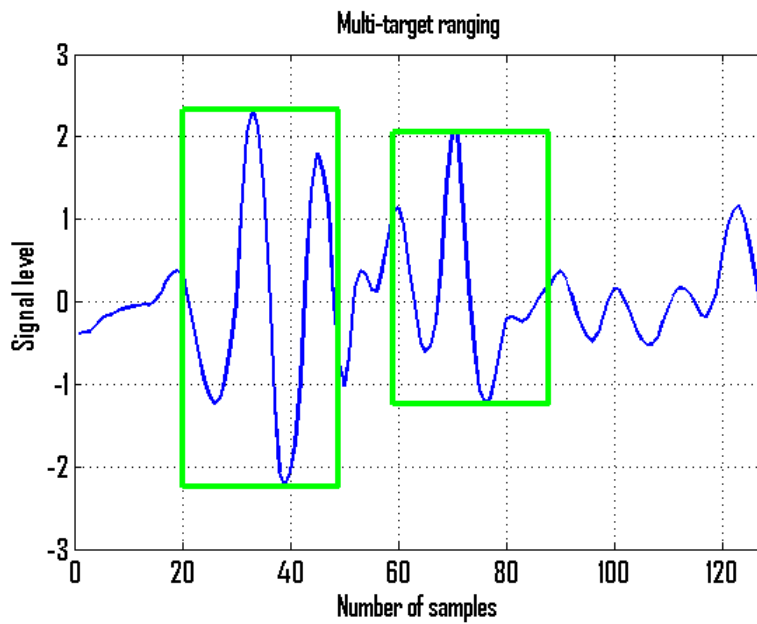


Figure 6.8.: Multiple target ranging

6.3.4. Tracking

Tracking

In Figure 6.9 and 6.9, the interface of one and two dimensional tracking are shown respectively. Figure 6.10 is the window that shows up during the tracking process. The green window indicates the position of the target in real time. The final result of position and velocity estimation can be also displayed by clicking the button 'Show Kalman Result'.

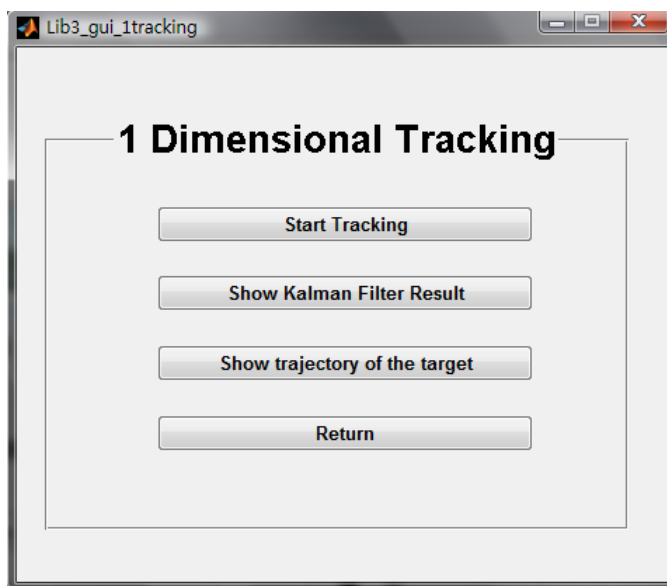


Figure 6.9.: The user interface for one dimensional tracking. Figure 6.10 pops up by clicking 'Start Tracking' which shows the tracking result in real time. The front edge of the green box indicates the pulse location. The 'Show Kalman Filter Result' gives the results of estimation of position and velocity as in Figure fig:1dkf.

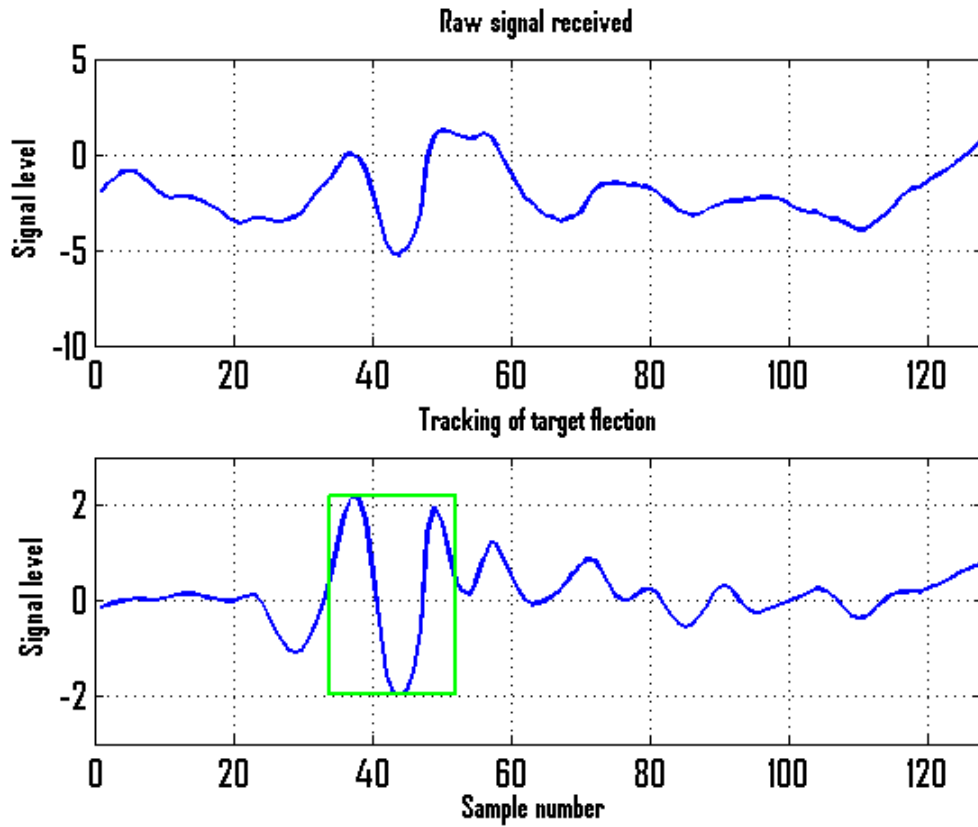
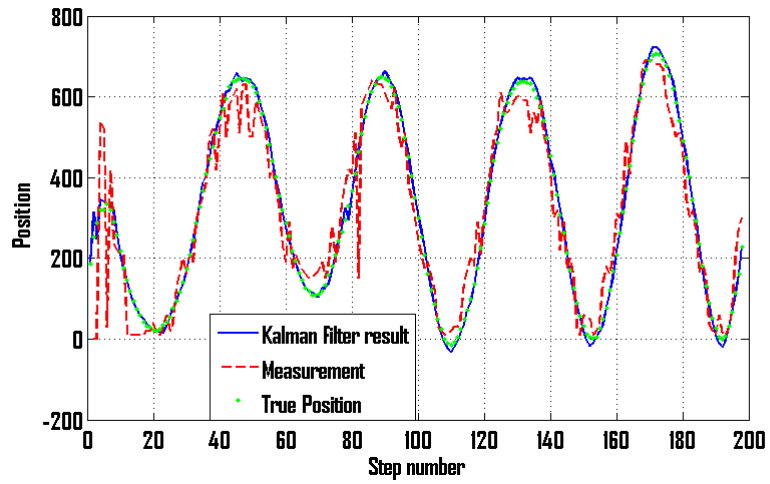
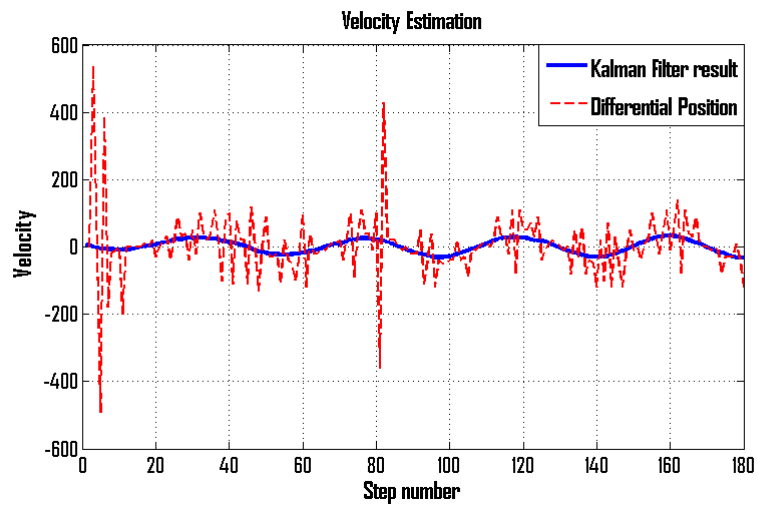


Figure 6.10.: The signals shown for one dimensional tracking in real time. The upper window shows the raw data without any processing, while the lower figure plots the signal after clutter removal and real time pulse locating. The starting edge of the green window indicates the location of the target in terms of number of samples.



(a) Position Estimation



(b) Velocity Estimation

Figure 6.11.: The position and velocity estimation from Kalman Filter.

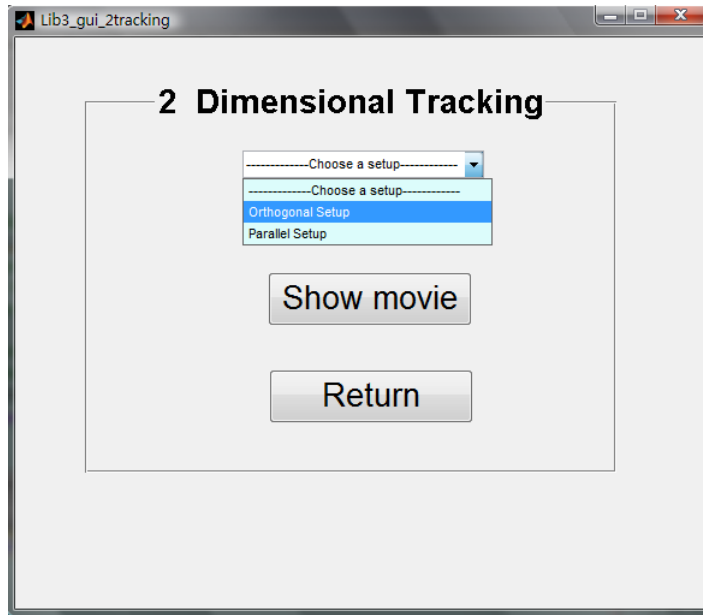
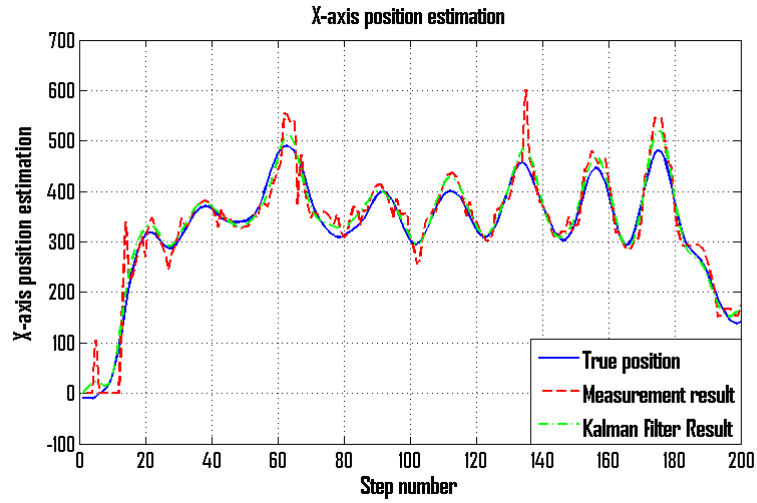
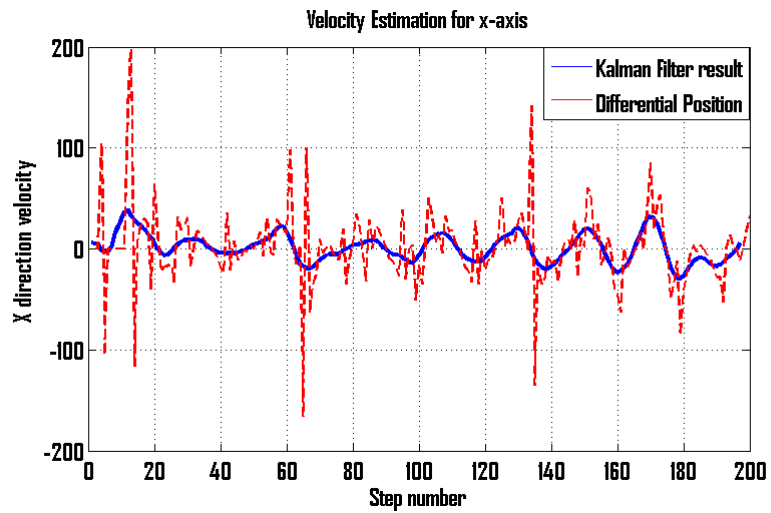


Figure 6.12.: The user interface for two dimensional tracking. The results from Kalman Filter estimation for both x and y axis are shown in Figure 6.13 and 6.14.

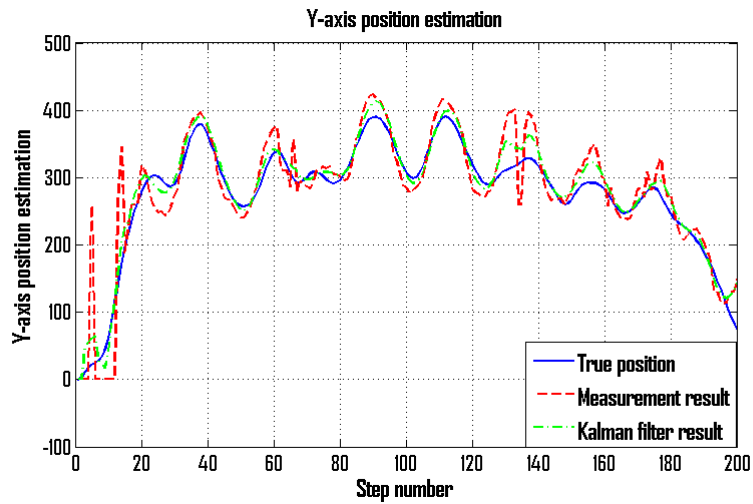


(a) Position Estimation

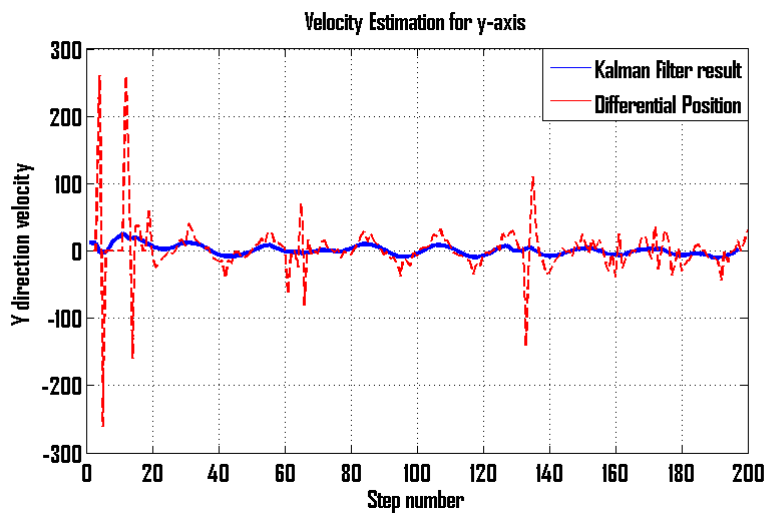


(b) Velocity Estimation

Figure 6.13.: The position and velocity estimation along x-axis by Kalman Filter.



(a) Position Estimation



(b) Velocity Estimation

Figure 6.14.: The position and velocity estimation along y-axis by Kalman Filter.

7. Conclusion and future work

In this thesis, we have mainly developed and implemented the classic radar functionalities, namely ranging and tracking according to the signal model we have established. One important pre-processing is the clutter map estimation which gives an optimal solution from a Frobenius norm point of view. The STFT based ranging method gives the best trade-off between complexity and estimation precision and is therefore used as real time pulse locating technique in tracking applications. A user interface has been implemented for the purpose of demonstration. This is the first step of algorithm design and functionality development for this prototype and the future work can focus on two directions: first, antenna array signal processing algorithm design; second, pulse signature analysis. The antenna array provides more features to the received signals from the targets. One applicable technique is Independent Component Analysis for signal separation in such cases. The signature analysis is potentially useful for target identification because the sensitivity of the signal and the large bandwidth result in signature variation according different targets. Since the developed algorithms are practically evaluated and ready to be implemented as a real product, the commercial potential is also under consideration.

References

- [1] Novelda, *Novelda R2A Ultra-wide band sensor user guide*, Oslo, Norway, 2008
- [2] R. Abrahamsson, J. Einarsson, J. Goop, E. Larsson, *Antenna design and application development for ultra-wideband-radar BS*. Swedish. thesis, Chalmers University of Technology, Gothenburg, Sweden, Feb. 2009.
- [3] Alan J. Laub, *Matrix Analysis for Scientists and Engineers*, Society for Industrial and Applied Mathematics; December 1, 2004
- [4] A. Farina, *Introduction to Radar Signal Data Processing: The Opportunity*, SELEX SISTEMI INTEGRATI, Rome, Italy, 2006
- [5] Yang Jin, Zhi Yong Hao, *Gaussian Window of Optimal Time-Frequency Resolution in Numerical Implementation of Short-Time Fourier Transform*, Applied Mechanics and Materials, Volumes 48-49, pp. 555-560, 2011
- [6] S. Haykin, *Neural Networks and Learning Machines (3rd Edition)*, Prentice Hall; 3 edition, November 28, 2008
- [7] P. S. Neelakanta, R. Sudhakar and D. DeGroff : *Langevin machine: a neural network based on stochastically justifiable sigmoidal function* , Biological Cybernetics, Volume 65, Number 5, 331-338, 1991
- [8] David L. Donoho and Yaakov Tsaig, *Fast Solution of 1-norm Minimization Problems, When the Solution May be Sparse*, Information Theory, IEEE Transactions, Volume 54, pp. 4789 - 4812, October 2008
- [9] Brown, R. G. and P. Y. C. Hwang: *Introduction to Random Signals and Applied Kalman Filtering*, Second Edition, John Wiley Sons, Inc., 1992.

A. Kalman filter for 2D tracking

A.1. Initialization

- State x is formed by position and velocity:

$$x_k = [p_x, p_y, \dot{p}_x, \dot{p}_y]^T \quad (\text{A.1})$$

p_x and p_y indicates the pulse location of x and y coordinate respectively.

- Observation is given by measured position:

$$z_k = [zx_k, zy_k] \quad (\text{A.2})$$

- Error covariance matrix:

$$\mathbf{P}_{0|0} = \begin{bmatrix} A & 0 & 0 & 0 \\ 0 & B & 0 & 0 \\ 0 & 0 & C & 0 \\ 0 & 0 & 0 & D \end{bmatrix} \quad (\text{A.3})$$

where the entries are chosen practically as:

$$[A \ B \ C \ D] = [3 \ 3 \ 1 \ 1]. \quad (\text{A.4})$$

- Observation noise v_k :

v_k is estimated from the measurements and assumed to be zero mean Gaussian white noise with covariance R_k .

$$\mathbf{v}_k \sim N(0, \mathbf{R}_k) \quad (\text{A.5})$$

- Process noise w_k :

w_k is assumed to be zero mean Gaussian white noise with covariance Q_k .

$$\mathbf{w}_k \sim N(0, \mathbf{Q}_k) \quad (\text{A.6})$$

- Step size and transfer matrix:
Transfer function F with step size T is given by:

$$F = \begin{bmatrix} 1 & 0 & T & 0 \\ 0 & 1 & 0 & T \\ 0 & 0 & 1 & 0 \\ 0 & 0 & 0 & 1 \end{bmatrix} \quad (\text{A.7})$$

- Observation matrix C:
C represents the relation between the true state x_k and measurement z_k . Here since the transform is just a matter of noise, C is initialized as:

$$C = \begin{bmatrix} 1 & 0 & 0 & 0 \\ 0 & 1 & 0 & 0 \end{bmatrix} \quad (\text{A.8})$$

A.2. Kalman equation

Kalman update for this application is summarized as follows:

- Prediction of error covariance:

$$\mathbf{P}_{k|k-1} = \mathbf{F}\mathbf{P}_{k-1|k-1}\mathbf{F}^T + \mathbf{Q}_k \quad (\text{A.9})$$

- Compute innovation covariance:

$$\mathbf{S}_k = \mathbf{C}\mathbf{P}_{k|k-1}\mathbf{C}^T + \mathbf{R}_k \quad (\text{A.10})$$

- Kalman's gain:

$$\mathbf{K}_k = \mathbf{P}_{k|k-1}\mathbf{C}^T\mathbf{S}_k^{-1} \quad (\text{A.11})$$

- Prediction of state estimation:

$$\mathbf{x}_{k|k-1} = \mathbf{F}\mathbf{x}_{k|k-1} \quad (\text{A.12})$$

- Prediction of observation:

$$\mathbf{z}_{k|k-1} = \mathbf{C}\mathbf{x}_{k|k-1} \quad (\text{A.13})$$

- State estimation update:

$$\hat{\mathbf{x}}_{k|k} = \hat{\mathbf{x}}_{k|k-1} + \mathbf{K}_k(\mathbf{z}_k - \mathbf{z}_{k|k-1}) \quad (\text{A.14})$$

- Error covariance update:

$$\mathbf{P}_{k|k} = (\mathbf{I} - \mathbf{K}_k\mathbf{C})\mathbf{P}_{k|k-1} \quad (\text{A.15})$$